FORCE Schemes on Unstructured Meshes II: Nonconservative Hyperbolic Systems

Michael Dumbser [a] Arturo Hidalgo [b] Manuel Castro [c]
Carlos Parés [c] Eleuterio F. Toro [a]

[a] *Laboratory of Applied Mathematics, University of Trento, Via Mesiano 77, I-38100 Trento, Italy*

[b] *ETSI Minas, Universidad Politécnica de Madrid, Calle Ríos Rosas 21, E-28003 Madrid, Spain*

[c] *Department of Mathematical Analysis, University of Málaga Campus Teatinos s/n, E-29080 Málaga, Spain*

Abstract

In this paper we propose a new high order accurate *centered* path-conservative method on unstructured triangular and tetrahedral meshes for the solution of multi-dimensional *non-conservative* hyperbolic systems, as they typically arise in the context of compressible multi-phase flows. Our path-conservative centered scheme is an extension of the centered method recently proposed in [36] for conservation laws, to which it reduces if the system matrix is the Jacobian of a flux function. The main advantage in the proposed centered approach compared to upwind methods is that no information about the eigenstructure of the system or Roe averages are needed. The final fully discrete high order accurate formulation in space and time is obtained using the general framework of $P_N P_M$ schemes proposed in [15], which unifies in one single general family of schemes classical finite volume and discontinuous Galerkin methods. We show applications of our high order centered method to the two- and three-dimensional Baer-Nunziato equations of compressible multiphase flows [3].

Key words: Non-conservative hyperbolic systems, centered schemes, unstructured meshes, high order finite volume and discontinuous Galerkin methods, compressible multi-phase flow, Baer–Nunziato model

Email addresses: michael.dumbser@ing.unitn.it (Michael Dumbser), arturo.hidalgo@upm.es (Arturo Hidalgo), castro@anamat.cie.uma.es (Manuel Castro), pares@anamat.cie.uma.es (Carlos Parés), toro@ing.unitn.it (Eleuterio F. Toro).

1 Introduction

Compressible multi-phase flows, such as liquid-vapor and solid-gas flows are encountered in numerous natural processes, such as sediment transport, meteorological flows, underwater volcano explosions or astrophysical flows. They also play a major role in many industrial applications arising in petrol, automotive, aerospace and chemical industry, in nuclear reactors or in paper and food manufacturing. Due to their wide applicability, these flows have attracted a lot of attention and have been the subject of intense research efforts over the years. However, the physical and mathematical modeling of compressible multi-phase flows is very challenging due to the complex nature of the interactions between the two phases and up to now no universally accepted multi–phase model is available. Many of the existing multi-phase models can *not* be expressed in the usual conservative form of a balance law

$$\frac{\partial}{\partial t} W + \nabla \cdot \underline{\underline{F}}(W) = S(W), \tag{1}$$

with W the vector of conserved variables, $\underline{\underline{F}}(W) = (f(W), g(W), h(W))$ the flux tensor and $S(W)$ an algebraic source term that can model other physical effects such as reaction or friction. Instead, there are important non-conservative terms that model the interaction between the phases that require a more general and non-conservative formulation of the governing PDE system. Hence, the models are more conveniently rewritten in the following general quasi-linear form

$$\frac{\partial}{\partial t} W + \underline{\underline{A}}(W) \cdot \nabla W = S(W), \tag{2}$$

where W and $S(W)$ have the same meaning as in (2) and where $\underline{\underline{A}}(W) = (A(W), B(W), C(W))$ is the so-called system matrix. We use block-matrix syntax to obtain a compact and simple notation of the matrices $A(W)$, $B(W)$ and $C(W)$ in the x, y and z directions, respectively. The discretization of a non-conservative system of the form (2) requires special care in the design of a numerical scheme. In particular, when $\underline{\underline{A}}$ is the Jacobian of a flux $\underline{\underline{F}}$, then (2) reduces to a classical balance law (1) and we therefore we want the numerical scheme to reduce to a fully conservative method in this case.

Since the classical Rankine-Hugoniot relations of a conservation law (1) for an isolated discontinuity moving in direction $\vec{n}$ at speed σ,

$$\sigma \left(W_R - W_L \right) = \Big(\underline{\underline{F}}(W_R) - \underline{\underline{F}}(W_L) \Big) \cdot \vec{n}, \tag{3}$$

are not applicable to a non-conservative system of the form (2), one has to introduce a more general definition of Rankine-Hugoniot relations that are also valid for (2). This has been achieved within the recent theory of Dal

Maso, LeFloch and Murat [25], called DLM theory in the following, which led to significant progress, both, on the theoretical side as well as concerning numerical algorithm development for non-conservative hyperbolic systems like (2). The DLM theory defines the weak solutions of (2) introducing a path $\mathbf{\Psi} = \mathbf{\Psi}(W_L, W_R, s)$ that connects the left and right state W_L and W_R, respectively, in phase-space across a discontinuity. As a consequence, the weak solution of the non-conservative system (2) then also depends on the choice of the path $\mathbf{\Psi}$. With the unit tensor $\mathbf{I}$ the resulting generalized Rankine-Hugoniot conditions for an isolated discontinuity traveling in direction $\vec{n}$ with speed σ read

$$0 = \int_{s=0}^{1} \left(\underline{\underline{A}}(\mathbf{\Psi}(W_L, W_R, s)) \cdot \vec{n} - \sigma \mathbf{I} \right) \frac{\partial \mathbf{\Psi}}{\partial s} ds. \tag{4}$$

From (4) it is obvious that for conservative systems, the DLM theory reproduces the classical Rankine-Hugoniot conditions across discontinuities (3), independent of the choice of $\mathbf{\Psi}$.

Very recently, the DLM theory has also been used as the basis of new numerical methods for non-conservative PDE, the so-called path-conservative schemes of Parés [28] and Castro et al. [10]. The generalized Roe schemes introduced by Toumi in [37] constitute a particular case of path-conservative methods. This framework has been used in several papers to design high order numerical methods in one and two space dimensions, both in the the finite volume framework, see e.g. [10], [21], [26], [9], [12], [8], [7] and in the discontinuous Galerkin finite element framework, see [29]. The extension to better than second order accurate ADER schemes on triangular meshes in has been achieved in [16] for the two-dimensional case. However, to our knowledge, up to now there exists no better than second order accurate path-conservative scheme on unstructured tetrahedral meshes in *three* space dimensions.

The development of such schemes is the aim of the present article, using a fully *centered* approach that does not need any additional information on the governing PDE (2) except for some evaluations of $\underline{\underline{A}}(W)$. In all the above-mentioned previous publications only *upwind* methods have been used to discretize the jump terms across the element boundaries. Castro and Parés use Roe-type schemes, whereas Rhebergen et al. use a non-conservative version of the HLLC method. All of these schemes need at least to some extent some information about the structure of the solution of the Riemann problem at the element interface. The most information is needed for the Roe-type Riemann solvers, less information is needed for HLLC. In this article, however, we propose a genuinely *centered* scheme, which only needs information about the time step, the geometry and simple evaluations of the system matrix $\underline{\underline{A}}(W)$.

The structure of the present article is as follows: In section 2 we present our high order accurate *centered* scheme on unstructured meshes based on the

general $P_N P_M$ reconstruction operator and the one-step time-discretization introduced in [15].
The system of governing equations under consideration in the present article, namely the multi-dimensional Baer-Nunziato model of compressible multi-phase flow [3], is described in section 3, where we also prove numerically the pressure non-disturbing condition (Abgrall condition) for a material interface at constant pressure and uniform velocity, see [31]. In order to show the high order of accuracy of our centered methods in space and time we invent a new *unsteady* and *genuinely multi-dimensional* test case with *exact analytical solution* for this model. To our knowledge, such a solution has not been presented anywhere else in literature before. Finally, in section 5, we present the first computations of better than second order of accuracy on unstructured triangular and tetrahedral meshes ever done for the Baer-Nunziato equations.

2 Numerical Method

2.1 The $P_N P_M$ Reconstruction Operator on Unstructured Meshes

Following the philosophy of Kolgan [24] and van Leer [38], higher order accurate Godunov-type finite volume schemes can be obtained using a reconstruction operator on the cell averages to obtain a piecewise linear data representation, which is then used for the flux computation. The idea of reconstruction was extended to even higher order of accuracy and general unstructured meshes in the pioneering work of Barth and Frederickson [5], who introduced the k-exact least-squares recovery operator. A completely different approach to obtain high order of accuracy in space was introduced for multi-dimensional nonlinear hyperbolic systems by the Runge-Kutta discontinuous Galerkin finite element approach of Cockburn and Shu [13], where the full polynomial (i.e. all its expansion coefficients) is evolved in time rather than only cell averages, like in the FV framework. This avoids the often cumbersome reconstruction step and yields a numerical method with spectral-like resolution properties. Recently, Dumbser et al. [15] proposed to generalize the k-exact least-squares reconstruction operator of Barth and Frederickson also to the DG finite element framework, obtaining a unified family of numerical schemes, called $P_N P_M$ methods, that contain high order FV and DG schemes only as special cases. There, the index N stands for the original polynomial degree that is used for representing the data in each cell and the index $M \geq N$ represents the degree of the reconstruction polynomial that is used for flux and source computation. $N = 0$ reproduces the standard finite volume scheme and the special case $M = N$ yields the usual DG finite element method. The $P_N P_M$ reconstruction operator is a direct extension of the algorithms proposed in [18,19] for finite volume schemes. For details, we refer the reader to the above mentioned

publications and give only a short review in this section. The computational domain Ω is discretized by conforming elements T_i, indexed by a single mono-index i ranging from 1 to the total number of elements N_E. The elements are chosen to be triangles in 2D and tetrahedrons in 3D. The union of all elements is the triangulation or tetrahedrization of the domain, respectively,

$$\mathcal{T}_\Omega = \bigcup_{i=1}^{N_E} T_i. \tag{5}$$

At the current time t^n the numerical solution u_h of (2) for the state vector W is stored in each cell under the form of piecewise polynomials of degree N from the space V_h, spanned by the basis functions $\Phi_l = \Phi_l(\vec{x})$, i.e. at $t = t^n$ we have for each element

$$u_h(\vec{x}, t^n) = \sum_l \Phi_l(\vec{x}) \hat{u}_l^n. \tag{6}$$

From u_h one then reconstructs piecewise polynomials w_h of degree $M \geq N$ from the space W_h, spanned by the basis functions $\Psi_l = \Psi_l(\vec{x})$. Following [15] the Ψ_l form an orthogonal basis and are identical with the Φ_l up to polynomial degree N. When reconstructing w_h for element T_i, we use the reconstruction stencil

$$\mathcal{S}_i = \bigcup_{k=1}^{n_e} T_{j(k)} \tag{7}$$

containing n_e elements. k is a local index that counts the elements in the stencil and $j = j(k)$ is the mapping from the local index k to the global indexation of the elements in $\mathcal{T}_\Omega$. For simplicity we now will only write j instead of $j(k)$.

The final numerical scheme proposed in this article relies essentially on the following three scalar products:

$$\langle f, g \rangle_{T_i} = \int_{t^n}^{t^{n+1}} \int_{T_i} (f(\vec{x}, t) \cdot g(\vec{x}, t))\, dV\, dt, \tag{8}$$

$$[f, g]_{T_i}^t = \int_{T_i} (f(\vec{x}, t) \cdot g(\vec{x}, t))\, dV, \tag{9}$$

$$\{f, g\}_{\partial T_i} = \int_{t^n}^{t^{n+1}} \int_{\partial T_i} (f(\vec{x}, t) \cdot g(\vec{x}, t))\, dS\, dt. \tag{10}$$

The first one denotes the scalar product of two functions f and g over the space-time element $T_i \times [t^n; t^{n+1}]$. The second one is the classical spatial scalar product at time t over the spatial element T_i, and the third one is a scalar product over the space-time boundary element $\partial T_i \times [t^n; t^{n+1}]$. Throughout the paper the operators $\langle f, g \rangle$ and $[f, g]^t$, written without the index T_i, denote

scalar products on the space-time reference element $T_E \times [0;1]$ and on the spatial reference element T_E at time t, respectively. The spatial reference element T_E is defined as the unit simplex with vertices $(0,0)$, $(1,0)$, $(0,1)$ in two space dimensions and vertices $(0,0,0)$, $(1,0,0)$, $(0,1,0)$ and $(0,0,1)$ in three space dimensions, respectively.

The piecewise reconstruction polynomial w_h of degree M is obtained from the piecewise polynomials u_h of degree N via a classical L_2-projection for all elements T_j in the stencil $\mathcal{S}_i$ as follows:

$$[\Phi_k, w_h]_{T_j}^{t^n} = [\Phi_k, u_h]_{T_j}^{t^n}, \qquad \forall T_j \in \mathcal{S}_i. \tag{11}$$

As in the work of Barth and Frederickson [5] the number of elements in the stencil must be chosen *larger* than the required number of degrees of freedom of w_h. Eqn. (11) thus leads to an *overdetermined* linear algebraic equation system for the expansion coefficients of w_h. It can be easily solved using a constrained least squares technique. The constraint is that Eqn. (11) is exactly satisfied for T_i. The integrals in (11) are computed using standard multidimensional Gaussian quadrature formulae of appropriate order [33]. For test problems with discontinuities, monotonicity is obtained for the finite volume version of the schemes (P_0P_M) using the WENO algorithm proposed in [18,19], but any of the other unstructured ENO/WENO algorithms available in literature [1,23,40] can be used as well.

2.2 The Local Space-Time Galerkin Predictor

The MUSCL scheme of van Leer [38] contains as a key ingredient the evolution stage of the reconstruction polynomial to the half time level. This makes the scheme second order accurate in time and linearly stable, in contrast to the first order in time second order in space scheme of Kolgan [24]. A better than second order accurate time evolution was first achieved by Harten et al. [22] in their original paper on ENO schemes using the semi-analytical Cauchy-Kovalewski procedure that requires successive differentiations of the governing PDE with respect to time and space. The main disadvantage with respect to the second order time-evolution proposed by van Leer was that the Cauchy-Kovalewski procedure needs explicit differentiation, whereas the van Leer time stepping only needs flux evaluations. The same procedure was also used in the ADER methods published in e.g. [34,20]. A new time-evolution procedure, based on a local weak formulation in space-time that uses only pure flux evaluations and no explicit differentiations, was recently proposed in [17] and [15] for conservative hyperbolic systems and in [16] for the non-conservative case. In this paper we only briefly give the extension of the method to the non-conservative case in three space dimensions:

We first introduce a space-time reference element $T_E \times [0;1]$ with $\vec{\xi} = (\xi, \eta, \zeta)$, in which ∇_ξ will denote the nabla operator with respect to reference coordinates. Starting then from PDE (2) in its strong form and transforming it into reference coordinates $(\vec{\xi}, \tau)$, we have:

$$\frac{\partial}{\partial \tau} W + \underline{\underline{A}}^* \cdot \nabla_\xi W = S^*. \tag{12}$$

The modified system matrices and the modified source term in the reference system are then given by

$$\underline{\underline{A}}^* := \Delta t \, \underline{\underline{A}}(W) J^T, \qquad S^* := \Delta t S(W), \qquad J = \frac{\partial \vec{\xi}}{\partial \vec{x}}. \tag{13}$$

After multiplying Eqn. (12) by a space-time test function $\theta_k = \theta_k(\xi, \eta, \zeta, \tau)$ from the space of piecewise space-time polynomials of degree M and integrating over the space-time control volume $T_E \times [0;1]$ one obtains

$$\left\langle \theta_k, \frac{\partial}{\partial \tau} \mathcal{W}_h \right\rangle + \left\langle \theta_k, \underline{\underline{A}}^* \cdot \nabla_\xi \mathcal{W}_h \right\rangle = \left\langle \theta_k, S^* \right\rangle. \tag{14}$$

We make the ansatz

$$\mathcal{W}_h = \mathcal{W}_h(\xi, \eta, \zeta, \tau) = \sum_l \theta_l(\xi, \eta, \zeta, \tau) \widehat{\mathcal{W}}_l := \theta_l \widehat{\mathcal{W}}_l, \tag{15}$$

$$\underline{\underline{A}}^* \cdot \nabla_\xi \mathcal{W}_h := \theta_l \, \widehat{\underline{\underline{A}}^* \nabla_\xi \mathcal{W}_l}, \qquad S^* := \theta_l \, \widehat{S_l^*}. \tag{16}$$

for the numerical solution $\mathcal{W}_h$, the non-conservative products $\underline{\underline{A}}^* \cdot \nabla_\xi \mathcal{W}_h$ and the source term S^*. In the whole paper we use the Einstein summation convention over two identical indices. For θ_k a nodal space-time basis is used, see [15], which is computationally cheaper than L_2-projection based on Gaussian quadrature. This means that source and non-conservative product are evaluated point-wise at each node, see [16]. We then insert (15) and (16) into (14) and obtain the following final fixed-point iteration scheme in order to evolve the reconstruction polynomials w_h in time within the predictor step of our one-step scheme:

$$\left\langle \theta_k, \frac{\partial}{\partial \tau} \theta_l \right\rangle \widehat{\mathcal{W}}_l^{i+1} = \left\langle \theta_k, \theta_l \right\rangle \left(\widehat{S_l^*}^i - \widehat{\underline{\underline{A}}^* \nabla_\xi \mathcal{W}_l}^i \right). \tag{17}$$

The initial condition w_h at relative time $\tau = 0$ (physical time $t = t^n$) is included in the usual way as for standard continuous Galerkin finite element methods. For details, also on the initial guess, see [15], where the coefficient vector $\widehat{\mathcal{W}}_l$ is appropriately split into degrees of freedom at time $\tau = 0$ and the others, so that w_h can be directly imposed for all nodes at $\tau = 0$. For the case of stiff source terms, we refer the reader to [16] and [17].

The fully discrete one-step form of the proposed path-conservative *centered* $P_N P_M$ schemes is obtained using the FORCE methodology presented in [35] and [36] for conservation laws in one and multiple space dimensions, respectively. Applying the operator $\langle \Phi_k, \cdot \rangle_{T_i}$ to PDE (2) yields

$$\left\langle \Phi_k, \frac{\partial}{\partial t} W \right\rangle_{T_i} + \left\langle \Phi_k, \underline{\underline{A}}(W) \cdot \nabla W \right\rangle_{T_i} = \langle \Phi_k, S(W) \rangle_{T_i} . \tag{18}$$

The first term in Eqn. (18) is approximated using instead of W the polynomials u_h from the space V_h and then integration by parts is performed in time. In all the other terms of Eqn. (18) the vector W is approximated by the solution $\mathcal{W}_h$ of the local space-time Galerkin predictor of section 2.2. The jumps in $\mathcal{W}_h$ at the element boundaries are resolved by a path-conservative method that defines a *weak derivative* in the sense of a Borel measure. Hence, we obtain the following family of fully discrete one-step ADER $P_N P_M$ scheme for PDE (2), where the jump term $\mathcal{D}^-(\mathcal{W}_h^-, \mathcal{W}_h^+, \vec{n})$ still remains to be defined:

$$\begin{aligned} \left[\Phi_k, u_h^{n+1} \right]_{T_i}^{t^{n+1}} - [\Phi_k, u_h^n]_{T_i}^{t^n} + \left\langle \Phi_k, \underline{\underline{A}}(\mathcal{W}_h) \cdot \nabla \mathcal{W}_h \right\rangle_{T_i \setminus \partial T_i} \\ + \left\{ \Phi_k, \mathcal{D}^-(\mathcal{W}_h^-, \mathcal{W}_h^+, \vec{n}) \right\}_{\partial T_i} = \langle \Phi_k, S(\mathcal{W}_h) \rangle_{T_i} , \end{aligned} \tag{19}$$

Here, $\mathcal{W}_h^-$ denotes the boundary extrapolated data from within element T_i and $\mathcal{W}_h^+$ denotes the boundary extrapolated data from the neighbor, respectively.

$\mathcal{D}^-$ is now a function so that:

- For every W, $\vec{n}$
$$\mathcal{D}^-(W, W, \vec{n}) = 0. \tag{20}$$
- For every $\mathcal{W}_h^-$, $\mathcal{W}_h^+$, $\vec{n}$:

$$\mathcal{D}^-(\mathcal{W}_h^-, \mathcal{W}_h^+, \vec{n}) + \mathcal{D}^-(\mathcal{W}_h^+, \mathcal{W}_h^-, -\vec{n}) = \int_0^1 \left(\underline{\underline{A}}(\mathbf{\Psi}(\mathcal{W}_h^-, \mathcal{W}_h^+, s)) \cdot \vec{n} \right) \frac{\partial \mathbf{\Psi}}{\partial s} ds. \tag{21}$$

Throughout this paper, we define the path $\mathbf{\Psi}$ by the family of segments

$$\mathbf{\Psi} = \mathbf{\Psi}(\mathcal{W}_h^-, \mathcal{W}_h^+, s) = \mathcal{W}_h^- + s(\mathcal{W}_h^+ - \mathcal{W}_h^-). \tag{22}$$

With this choice, the generalized Roe property for defining a Roe-type matrix

in the non-conservative case (see [10],[28])

$$\left(\tilde{\underline{\underline{A}}}_{\mathbf{\Psi}}(\mathcal{W}_h^-,\mathcal{W}_h^+)\cdot\vec{n}\right)\left(\mathcal{W}_h^+-\mathcal{W}_h^-\right)=\int_0^1\left(\underline{\underline{A}}(\mathbf{\Psi}(\mathcal{W}_h^-,\mathcal{W}_h^+,s))\cdot\vec{n}\right)\frac{\partial\mathbf{\Psi}}{\partial s}ds, \quad (23)$$

simplifies to

$$\left(\tilde{\underline{\underline{A}}}_{\mathbf{\Psi}}(\mathcal{W}_h^-,\mathcal{W}_h^+)\cdot\vec{n}\right)=\int_0^1\left(\underline{\underline{A}}(\mathbf{\Psi}(\mathcal{W}_h^-,\mathcal{W}_h^+,s))\cdot\vec{n}\right)ds. \quad (24)$$

We would like to remark that in the *conservative* case, the generalized Roe property (23) reduces to the classical Roe property,

$$\left(\tilde{\underline{\underline{A}}}_{\mathbf{\Psi}}(\mathcal{W}_h^-,\mathcal{W}_h^+)\cdot\vec{n}\right)\left(\mathcal{W}_h^+-\mathcal{W}_h^-\right)=\left(\underline{\underline{F}}(\mathcal{W}_h^+)-\underline{\underline{F}}(\mathcal{W}_h^-)\right)\cdot\vec{n}, \quad (25)$$

independent of the path $\mathbf{\Psi}$.

The explicit computation of the path integral appearing in (24) can become very complicated or even impossible for general non-linear non-conservative systems. In [6] we therefore proposed an entirely *numerical* way of computing the path integral on the right hand side of (24) directly via Gaussian quadrature rules of suitably high order of accuracy. This purely numerical procedure does *not* require the explicit computation of the Roe averages, which becomes already quite difficult for the Euler equations of compressible gas dynamics, see [30]. Therefore, using a Gaussian quadrature rule with G points on the unit interval $I=[0;1]$, weights ω_i and positions μ_i, respectively (see [33]), we compute an *approximate Roe matrix* in normal direction as follows:

$$\tilde{A}_{\mathbf{\Psi}}^G:=\sum_{i=1}^G\omega_i\left(\underline{\underline{A}}(\mathbf{\Psi}(\mathcal{W}_h^-,\mathcal{W}_h^+,\mu_i))\cdot\vec{n}\right)\approx\left(\tilde{\underline{\underline{A}}}_{\mathbf{\Psi}}(\mathcal{W}_h^-,\mathcal{W}_h^+)\cdot\vec{n}\right). \quad (26)$$

The method given by Eqn. (26) is a simple and general *purely numerical* way of defining an approximate Roe matrix for any given hyperbolic system, independent of its complexity, without having to compute the Roe averages explicitly. This also holds in particular for conservative systems. Since our method directly starts from the definition of the generalized Roe matrix (23), the problems of existence and uniqueness of the Roe averages [37] does not arise. We emphasize that the numerical integration required in (26) can be done up to *arbitrary accuracy*, using e.g. Romberg extrapolation or other adaptive techniques. However we note in practical computations that normally the use of three Gaussian points in (26) is sufficient. The reader is encouraged to try more sophisticated adaptive integration techniques if necessary. Note that also Toumi [37] defined the Roe matrix by (23), but he used *analytical* integration along the path integral instead of the *numerical* quadrature used in Eqn. (26).

For the original Roe method, however, one needs to compute the absolute value of the matrix $\tilde{A}^G_{\mathbf{\Psi}}$, which requires the computation of all its eigenvectors and eigenvalues. Although this can be also done fully numerically using standard linear algebra packages, as it has been done e.g. in [10,16], in the present paper we considerably reduce computational effort by resorting to a purely *centered* approach that needs the approximate Roe matrix $\tilde{A}^G_{\mathbf{\Psi}}$ from (26), but that does *not* need its eigenstructure. The natural multi-dimensional extension of the non-conservative FORCE schemes developed in the one-dimensional case in [12,6] now follows in the same way as the extension of the conservative one-dimensional FORCE method of Toro and Billet [35] to multiple space dimensions presented in [36]. We consequently define the jump term $\mathcal{D}^-(\mathcal{W}_h^-, \mathcal{W}_h^+, \vec{n})$ as follows:

$$\mathcal{D}^-(\mathcal{W}_h^-, \mathcal{W}_h^+, \vec{n}) = \frac{1}{2}\left(\tilde{A}^G_{\mathbf{\Psi}} - \beta_j^{\mathrm{LW}}\left(\tilde{A}^G_{\mathbf{\Psi}}\right)^2 - \beta_j^{\mathrm{LF}}\mathbf{I}\right)\left(\mathcal{W}_h^+ - \mathcal{W}_h^-\right), \tag{27}$$

where $\mathbf{I}$ is the identity matrix and the two constants β_{LW} and β_{LF} contain only information on the geometry and the time step Δt, as derived in detail in [36]:

$$\beta_j^{\mathrm{LF}} = \frac{2}{\Delta t S_j}\frac{V_j^- V_j^+}{V_j^- + V_j^+}, \qquad \beta_j^{\mathrm{LW}} = \frac{1}{2}\frac{\Delta t S_j}{V_j^- + V_j^+}. \tag{28}$$

Here, $V_j^{\pm}$ denote the sub-volumes defined at each edge/face j, where V_j^- is the sub-volume inside the considered element and V_j^+ is the corresponding sub-volume in the neighbor adjacent to edge j, see Fig. 1 for the 2D case. The subvolumes are constructed connecting the vertices of an edge/face with the barycenter of the element. Obviously, we have $\sum V_j = |T_i|$. With $S_j = |\partial T_j|$ we denote the length/area of edge/face number j.

We recall that according to [15] the conservative equivalent of the $P_N P_M$ scheme (19) in order to solve conservation laws of the form (1) is given by

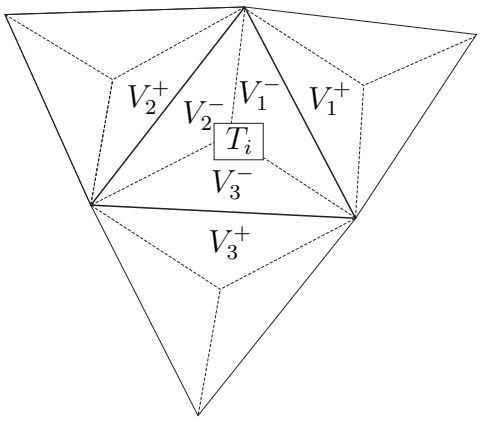

Fig. 1. Notation for the definition of $V_j^{\pm}$ on unstructured triangular meshes.

$$\left[\Phi_k, u_h^{n+1}\right]_{T_i}^{t^{n+1}} - \left[\Phi_k, u_h^n\right]_{T_i}^{t^n} - \left\langle \nabla\Phi_k \cdot \underline{\underline{F}}(\mathcal{W}_h)\right\rangle_{T_i\setminus\partial T_i} + \left\{\Phi_k, \mathcal{G}_{i+\frac{1}{2}}\right\}_{\partial T_i} = \left\langle \Phi_k, S(\mathcal{W}_h)\right\rangle_{T_i}, \tag{29}$$

with the numerical flux $\mathcal{G}_{i+\frac{1}{2}} = \mathcal{G}_{i+\frac{1}{2}}(\mathcal{W}_h^-, \mathcal{W}_h^+, \vec{n})$.

Since we want our path-conservative centered method to be conservative when (2) is a conservation law (1), i.e. when $\underline{\underline{A}}$ is the Jacobian of a flux $\underline{\underline{F}}$, we rewrite the scheme (19) under this assumption. The following identities hold in the conservative case:

$$\left\langle \Phi_k, \underline{\underline{A}}(\mathcal{W}_h)\cdot\nabla\mathcal{W}_h\right\rangle_{T_i\setminus\partial T_i} = \left\langle \Phi_k, \nabla\cdot\underline{\underline{F}}(\mathcal{W}_h)\right\rangle_{T_i\setminus\partial T_i} \tag{30}$$

and

$$\left\langle \Phi_k, \nabla\cdot\underline{\underline{F}}(\mathcal{W}_h)\right\rangle_{T_i\setminus\partial T_i} = \left\{\Phi_k, \underline{\underline{F}}(\mathcal{W}_h^-)\cdot\vec{n}\right\}_{\partial T_i} - \left\langle \nabla\Phi_k\cdot\underline{\underline{F}}(\mathcal{W}_h)\right\rangle_{T_i\setminus\partial T_i}. \tag{31}$$

Following [28], we define the numerical flux as

$$\mathcal{G}_{i+\frac{1}{2}} = \mathcal{G}(\mathcal{W}_h^-, \mathcal{W}_h^+, \vec{n}) := \underline{\underline{F}}(\mathcal{W}_h^-)\cdot\vec{n} + \mathcal{D}^-(\mathcal{W}_h^-, \mathcal{W}_h^+, \vec{n}), \tag{32}$$

where simple algebraic manipulations reveal that $\mathcal{G}_{i+\frac{1}{2}}$ satisfies the usual consistency requirements. Inserting Eqns. (32), (30) and (31) into Eqn. (19) yields directly the conservative P_NP_M scheme (29). Hence, the path-conservative P_NP_M method (19) reduces to the conservative P_NP_M scheme (29) in the case where the non-conservative PDE (2) is a system of conservation laws (1).
Furthermore, in this case the centered scheme (19) with the FORCE jump term (27) reduces to the conservative scheme (29), with the following flux function, see [36]:

$$\mathcal{G}_{i+\frac{1}{2}} = \frac{1}{2}\left(\mathcal{G}_{i+\frac{1}{2}}^{\mathrm{LW}'} + \mathcal{G}_{i+\frac{1}{2}}^{\mathrm{LF}'}\right), \tag{33}$$

with a generalized Lax-Wendroff-type flux

$$\mathcal{G}_{i+\frac{1}{2}}^{\mathrm{LW}'} = \frac{V_j^+\underline{\underline{F}}(\mathcal{W}_h^+) + V_j^-\underline{\underline{F}}(\mathcal{W}_h^-)}{V_j^- + V_j^+}\cdot\vec{n} - \frac{1}{2}\beta_j^{\mathrm{LW}}\tilde{A}_{\mathbf{\Psi}}^G\left(\underline{\underline{F}}(\mathcal{W}_h^+) - \underline{\underline{F}}(\mathcal{W}_h^-)\right)\cdot\vec{n}, \tag{34}$$

and a generalized Lax-Friedrichs-type flux

$$\mathcal{G}_{i+\frac{1}{2}}^{\mathrm{LF}'} = \frac{V_j^-\underline{\underline{F}}(\mathcal{W}_h^+) + V_j^+\underline{\underline{F}}(\mathcal{W}_h^-)}{V_j^- + V_j^+}\cdot\vec{n} - \frac{1}{2}\beta_j^{\mathrm{LF}}\,\mathbf{I}\left(\mathcal{W}_h^+ - \mathcal{W}_h^-\right). \tag{35}$$

3 The Baer-Nunziato Model for Compressible Multi-Phase Flow

The Baer-Nunziato model for compressible two-phase flow is given by the following system of equations, see [3,27]:

$$\left.\begin{aligned}
&\tfrac{\partial}{\partial t}\left(\phi_1\rho_1\right) + \nabla\cdot\left(\phi_1\rho_1\mathbf{u_1}\right) = 0,\\
&\tfrac{\partial}{\partial t}\left(\phi_1\rho_1\mathbf{u_1}\right) + \nabla\cdot\left(\phi_1\rho_1\mathbf{u_1}\otimes\mathbf{u_1}\right) + \nabla\phi_1 p_1 = p_I\nabla\phi_1 + \lambda\left(\mathbf{u_2}-\mathbf{u_1}\right),\\
&\tfrac{\partial}{\partial t}\left(\phi_1\rho_1 E_1\right) + \nabla\cdot\left(\left(\phi_1\rho_1 E_1 + \phi_1 p_1\right)\mathbf{u_1}\right) = -p_I\partial_t\phi_1 + \lambda\,\mathbf{u_I}\cdot\left(\mathbf{u_2}-\mathbf{u_1}\right),\\
&\tfrac{\partial}{\partial t}\left(\phi_2\rho_2\right) + \nabla\cdot\left(\phi_2\rho_2\mathbf{u_2}\right) = 0,\\
&\tfrac{\partial}{\partial t}\left(\phi_2\rho_2\mathbf{u_2}\right) + \nabla\cdot\left(\phi_2\rho_2\mathbf{u_2}\otimes\mathbf{u_2}\right) + \nabla\phi_2 p_2 = p_I\nabla\phi_2 - \lambda\,\left(\mathbf{u_2}-\mathbf{u_1}\right),\\
&\tfrac{\partial}{\partial t}\left(\phi_2\rho_2 E_2\right) + \nabla\cdot\left(\left(\phi_2\rho_2 E_2 + \phi_2 p_2\right)\mathbf{u_2}\right) = p_I\partial_t\phi_1 - \lambda\,\mathbf{u_I}\cdot\left(\mathbf{u_2}-\mathbf{u_1}\right),\\
&\tfrac{\partial}{\partial t}\phi_1 + \mathbf{u_I}\nabla\phi_1 = 0.
\end{aligned}\right\} \tag{36}$$

The system is closed by the so-called stiffened equation of state (EOS) for each phase:

$$e_k = \frac{p_k + \gamma_k\pi_k}{\rho_k(\gamma_k - 1)} \tag{37}$$

Here, ϕ_k denotes the volume fraction of phase k, ρ_k is the density, $\mathbf{u_k}$ is the velocity vector, $E_k = e_k + \frac{1}{2}\mathbf{u_k}^2$ and e_k are the phase specific total and internal energies, respectively, and λ is a parameter characterizing the friction between both phases. In the literature, phase 1 is also called the solid phase and phase 2 the gas phase. We will therefore use the subscripts 1 and s as well as 2 and g as synonyms in the following. For the interface velocity and pressure $\mathbf{u_I}$ and p_I we choose $\mathbf{u_I} = \mathbf{u_1}$ and $p_I = p_2$ respectively, according to [3,27], although other choices are possible, see e.g. the paper by Saurel and Abgrall [31]. The state vector W is

$$W = \left(\phi_1\rho_1,\ \phi_1\rho_1\mathbf{u}_1,\ \phi_1\rho_1 E_1,\ \phi_2\rho_2,\ \phi_2\rho_2\mathbf{u}_2,\ \phi_2\rho_2 E_2,\ \phi_1\right). \tag{38}$$

We can cast system (36) in the general non-conservative form (2) by defining the system matrix $\underline{\underline{A}}(W) = (A(W), B(W), C(W))$, where $A(W)$, $B(W)$ and $C(W)$ are the Jacobian matrices of the fluxes f, g and h given in (36) plus the contribution of the non-conservative products, the so-called nozzling terms. The system matrix $\underline{\underline{A}}(W)$ and the source term vector $S(W)$ can be readily computed from (36), so we do not need to show them here explicitly, to save space.

Verification of the Abgrall Condition. A very important condition that has to be satisfied by a numerical method for system (36) is the so-called

pressure non-disturbing condition or the *Abgrall condition* [31], which states that a mixture of two phases that moves with uniform velocity and pressure should exactly preserve the constant pressure. At this place we show the results of a very simple numerical experiment carried out with the first order version of the scheme in 2D to demonstrate that our jump term $\mathcal{D}^-$ automatically satisfies this property, although we are not able to demonstrate it analytically. The numerical test is performed on the domain $\Omega = [-1;1] \times [-1;1]$ with four periodic boundary conditions. Ω is discretized using 22476 triangles of characteristic mesh size $h = 0.01$. Phase 1 - the solid phase - is modeled using the stiffened EOS with parameters $\gamma_1 = 3$ and $\pi_1 = 2$, whereas the gas phase is modeled as usual by an ideal diatomic gas with $\gamma_2 = 1.4$ and $\pi_2 = 0$. Initially, the pressures and densities for both phases are $p_{1,2} = 1$, $\rho_1 = 10$ and $\rho_2 = 1$ everywhere and the uniform velocity field for both phases is given by $u_{1,2} = v_{1,2} = 1$. Within a circle of radius $R = 0.25$, centered in the origin, we then set the solid phase volume fraction to $\phi_s = \phi_1 = 1 - 10^{-14}$ and outside this circle we set it equal to $\phi_s = \phi_1 = 10^{-14}$. We then evolve the system for 780 time steps until $t = 2$, which corresponds to one entire advection period of the solid-gas interphase. The results obtained for the solid volume fraction ϕ_s are depicted in Fig. 2 (left, middle) and a one-dimensional cut along the x-axis through both pressure profiles at $t = 2.0$ is shown in Fig. 2 (right). The pressure non-disturbing condition is almost satisfied up to machine accuracy. Note that p is computed from the conserved variables W a posteriori, hence additional round-off errors are introduced. The L^∞ error for the solid pressure $p_s = p_1$ in this test case was 2.842E-012 and for the gas pressure $p_g = p_2$ the L^∞ error was 2.887E-015.

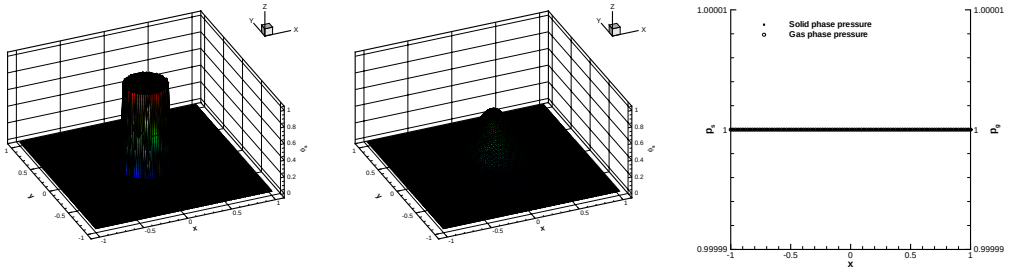

Fig. 2. Numerical verification of the Abgrall condition. Left: initial distribution of ϕ_s. Middle: distribution of ϕ_s after $t = 2$ using the first order version of our centered schemes (P_0P_0). Right: cut along the x-axis showing the solid and gas pressure profiles after $t = 2$. No unphysical spurious pressure oscillations are visible.

4 Numerical Convergence Studies

In this section we perform a numerical convergence test for the two-dimensional compressible Baer-Nunziato equations presented in section 3. The process fol-

lowed is analogous to the one described in [23] and [4], where convergence is assessed via the analytical solution of an isentropic vortex. The exact solution of this unsteady test case is obtained in two steps. First, one finds an exact stationary and rotationally symmetric solution of the governing PDE system that approaches a constant state as $r \to \infty$, in order to be compatible with periodic boundary conditions. Second, to make the test case unsteady, one uses the principle of Galilean invariance inherent in all governing equations based on Newtonian mechanics and superimposes a uniform velocity field to the solution found in step one. After one advection period through a periodic rectangular computational domain, the exact solution is then given by the initial condition.

To assess the accuracy of our method for the 2D Baer-Nunziato model, we first write the model equations using cylindrical coordinates $(r-\phi)$ as

$$
\left.
\begin{aligned}
&\tfrac{\partial}{\partial t}\left(\phi_1\rho_1\right)+\tfrac{1}{r}\left[\tfrac{\partial}{\partial r}\left(r\phi_1\rho_1u_1^r\right)+\tfrac{\partial}{\partial\phi}\left(\phi_1\rho_1u_1^\phi\right)\right]=0\ ,\\
&\tfrac{\partial}{\partial t}\left(\phi_1\rho_1\mathbf{u_1}\right)+\boldsymbol{\nu^r}\left[\tfrac{\partial}{\partial r}\left(\phi_1\rho_1\left(u_1^r\right)^2\right)+\tfrac{1}{r}\tfrac{\partial}{\partial\phi}\left(\phi_1\rho_1u_1^ru_1^\phi\right)+\tfrac{1}{r}\phi_1\rho_1\left(\left(u_1^r\right)^2-\left(u_1^\phi\right)^2\right)\right]\\
&+\boldsymbol{\nu^\phi}\left[\tfrac{\partial}{\partial r}\left(\phi_1\rho_1u_1^\phi u_1^r\right)+\tfrac{1}{r}\tfrac{\partial}{\partial\phi}\left(\phi_1\rho_1\left(u_1^\phi\right)^2\right)+\tfrac{2}{r}u_1^ru_1^\phi\right]\\
&+\boldsymbol{\nu^r}\tfrac{\partial}{\partial r}\left(\phi_1p_1\right)+\boldsymbol{\nu^\phi}\tfrac{1}{r}\tfrac{\partial}{\partial\phi}\left(\phi_1p_1\right)=p_I\left[\boldsymbol{\nu^r}\tfrac{\partial}{\partial r}\phi_1+\boldsymbol{\nu^\phi}\tfrac{1}{r}\tfrac{\partial}{\partial\phi}\phi_1\right]+\lambda\left(\mathbf{u_2}-\mathbf{u_1}\right)\ ,\\
&\tfrac{\partial}{\partial t}\left(\phi_1\rho_1E_1\right)+\tfrac{1}{r}\left[\tfrac{\partial}{\partial r}\left(r\phi_1\rho_1E_1u_1^r\right)+\tfrac{\partial}{\partial\phi}\left(\phi_1\rho_1E_1u_1^\phi\right)\right]+\tfrac{1}{r}\left[\tfrac{\partial}{\partial r}\left(r\phi_1p_1u_1^r\right)+\tfrac{\partial}{\partial\phi}\left(\phi_1p_1u_1^\phi\right)\right]\\
&=p_I\tfrac{\partial}{\partial t}\phi_1+\lambda\mathbf{u_I}\left(\mathbf{u_2}-\mathbf{u_1}\right)\\
&\tfrac{\partial}{\partial t}\left(\phi_2\rho_2\right)+\tfrac{1}{r}\left[\tfrac{\partial}{\partial r}\left(r\phi_2\rho_2u_2^r\right)+\tfrac{\partial}{\partial\phi}\left(\phi_2\rho_2u_2^\phi\right)\right]=0\ ,\\
&\tfrac{\partial}{\partial t}\left(\phi_2\rho_2\mathbf{u_2}\right)+\boldsymbol{\nu^r}\left[\tfrac{\partial}{\partial r}\left(\phi_2\rho_2\left(u_2^r\right)^2\right)+\tfrac{1}{r}\tfrac{\partial}{\partial\phi}\left(\phi_2\rho_2u_2^ru_2^\phi\right)+\tfrac{1}{r}\phi_2\rho_2\left(\left(u_2^r\right)^2-\left(u_2^\phi\right)^2\right)\right]\\
&+\boldsymbol{\nu^\phi}\left[\tfrac{\partial}{\partial r}\left(\phi_2\rho_2u_2^\phi u_2^r\right)+\tfrac{1}{r}\tfrac{\partial}{\partial\phi}\left(\phi_2\rho_2\left(u_2^\phi\right)^2\right)+\tfrac{2}{r}u_2^ru_2^\phi\right]\\
&+\boldsymbol{\nu^r}\tfrac{\partial}{\partial r}\left(\phi_2p_2\right)+\boldsymbol{\nu^\phi}\tfrac{1}{r}\tfrac{\partial}{\partial\phi}\left(\phi_2p_2\right)=p_I\left[\boldsymbol{\nu^r}\tfrac{\partial}{\partial r}\phi_2+\boldsymbol{\nu^\phi}\tfrac{1}{r}\tfrac{\partial}{\partial\phi}\phi_2\right]-\lambda\left(\mathbf{u_2}-\mathbf{u_1}\right)\ ,\\
&\tfrac{\partial}{\partial t}\left(\phi_2\rho_2E_2\right)+\tfrac{1}{r}\left[\tfrac{\partial}{\partial r}\left(r\phi_2\rho_2E_2u_2^r\right)+\tfrac{\partial}{\partial\phi}\left(\phi_2\rho_2E_2u_2^\phi\right)\right]+\tfrac{1}{r}\left[\tfrac{\partial}{\partial r}\left(r\phi_2p_2u_2^r\right)+\tfrac{\partial}{\partial\phi}\left(\phi_2p_2u_2^\phi\right)\right]\\
&=-p_I\tfrac{\partial}{\partial t}\phi_1-\lambda\mathbf{u_I}\left(\mathbf{u_2}-\mathbf{u_1}\right)\\
&\tfrac{\partial}{\partial t}\phi_1+\mathbf{u_I}\left(\boldsymbol{\nu^r}\tfrac{\partial}{\partial r}\phi_1+\boldsymbol{\nu^\phi}\tfrac{1}{r}\tfrac{\partial}{\partial\phi}\phi_1\right)=0.
\end{aligned}
\right\}
\tag{39}
$$

where u_k^ϕ are the velocities in angular direction and u_k^r are the velocities in radial direction. Furthermore, $\boldsymbol{\nu}^{\mathbf{r}}$ is the normal unity vector in radial direction while $\boldsymbol{\nu}^{\boldsymbol{\phi}}$ is the normal unity vector in angular direction. In order to obtain an analytical solution, we impose rotational symmetry ($\frac{\partial}{\partial\phi} = 0$) and neglect the effect of friction ($\lambda = 0$). We thus obtain the simplified system

$$\frac{\partial}{\partial r}\left(\phi_1 p_1\right) = p_2\frac{\partial}{\partial r}\phi_1 + \frac{1}{r}\left(u_1^\phi\right)^2\phi_1\rho_1\ ,\ \frac{\partial}{\partial r}\left(\phi_2 p_2\right) = p_2\frac{\partial}{\partial r}\phi_2 + \frac{1}{r}\left(u_2^\phi\right)^2\phi_2\rho_2\ . \tag{40}$$

System (40) is an nonlinear system of ODE in the two variables ϕ_1 and p_2 since $\phi_2 = 1 - \phi_1$ is known. In order to obtain a simple analytical solution, we prescribe ϕ_2 and p_2 and solve (40) for the two angular velocities u_1^ϕ and u_2^ϕ. For our particular test case, we choose for the pressures

$$p_k = p_{k0}\left(1 - \frac{1}{4}e^{\left(1 - r^2/s_k^2\right)}\right), \qquad (k = 1, 2)\ , \tag{41}$$

and for the volume fraction of the solid phase ϕ_1 we impose

$$\phi_1 = \frac{1}{3} + \frac{1}{2\sqrt{2\pi}}e^{-r^2/2}. \tag{42}$$

We then can finally solve (40) using (41) and (42) to compute the angular velocities of each phase as

$$u_1^\phi = \frac{1}{2s_1 D}\sqrt{rD\left[p_{10}\left(4\sqrt{2\pi}F_1 + 6H_1 - 12Gs_1^2 + 3H_1 s_1^2\right) + 3p_{20}s_1^2\left(4G - H_2\right)\right]}\ ,$$

$$u_2^\phi = \frac{r\sqrt{2}}{2\rho_2 s_2}\sqrt{\rho_2 p_{20} F_2}\ , \tag{43}$$

with

$$H_k = e^{-\frac{2r^2 + r^2 s_k^2 - 2s_k^2}{2s_k^2}}, \quad F_k = e^{-\frac{(r - s_k)(r + s_k)}{s_k^2}}, \quad (k = 1, 2),$$

and

$$G = e^{-r^2/2}, \qquad D = \rho_1\left(2\sqrt{2\pi} + 3G\right).$$

Once the rotationally symmetric stationary solution of the compressible Baer-Nunziato equations has been obtained, we can easily construct an *unsteady* solution using the principle of Galilean invariance of Newtonian mechanics by simply adding a constant uniform velocity field to both phases with velocity components $\bar{u}$ and $\bar{v}$. Using this analytical solution, we calculate the convergence rates of the numerical approach, using the following particular

data

$$\rho_1 = 1, \quad \rho_2 = 2, \quad p_{10} = 1, \quad p_{20} = \frac{3}{2}, \quad s_1 = \frac{3}{2}, \quad s_2 = \frac{7}{5}, \quad \bar{u} = \bar{v} = 2. \tag{44}$$

We solve the initial value problem on a square domain $\Omega = [-5;5] \times [-5;5]$ using unstructured triangular meshes with four periodic boundary conditions. The exact solution of the problem is given by the initial condition after $T = 5$. The results obtained with all kinds of $P_N P_M$ schemes are shown for the second conserved variable (x-momentum of the solid phase) at time $t = T$ in Table 1. We observe that all high order schemes reach their designed order of accuracy.

5 Applications

The test cases shown in this section have been selected to validate our high order centered approach on unstructured triangular and tetrahedral meshes in two and three space dimensions. To ensure a non-oscillatory behavior, the WENO reconstruction technique proposed in [18] and [19] has been employed. The Courant number is set in all 2D computations to 0.5 and in the 3D computations it is set to 0.4. The time step is computed based on the incircle and insphere diameters as characteristic length scales, respectively.

5.1 Shock Tube Problems in Multiple Space Dimensions

To validate our multi-dimensional numerical schemes for the compressible Baer-Nunziato equations we solve a set of originally 1D shock tube problems on unstructured meshes in 2D and 3D. For these shock tube problems, exact reference solutions are available in the literature [2,32,14]. To our knowledge, the first exact Riemann solver for the compressible Baer-Nunziato equations was published by Andrianov and Warnecke [2]. However, it was not a direct solver, but given two states in the star region, it computed backwards the corresponding initial conditions as well as the full wave structure. The purpose of this solver was to construct specific exact solutions to validate numerical methods. The first direct solver has been published by Schwendeman et al. in [32], who also constructed a Godunov method based on this Riemann solver. The non-conservative products have been incorporated using a thin layer analysis for the solid contact, from which subsequently the corresponding jump conditions have been derived. The most recent exact Riemann solver for the compressible Baer-Nunziato equations has been published by Deledicque and Papalexandris [14], who use a different approach than the one proposed in [32] to compute the exact solution of the Riemann problem. From the above mentioned articles we have chosen a set of six different Riemann problems, whose

Table 1. Numerical convergence study of $P_N P_M$ schemes from second to sixth order of accuracy in space and time applied to the two-dimensional Baer-Nunziato equations. Errors are shown for variable $\phi_1 \rho_1 u_1$.

N_G	L^2	$\mathcal{O}_{L^2}$	L^2	$\mathcal{O}_{L^2}$	L^2	$\mathcal{O}_{L^2}$	L^2	$\mathcal{O}_{L^2}$	L^2	$\mathcal{O}_{L^2}$	L^2	$\mathcal{O}_{L^2}$
$\mathcal{O}2$	P_0P_1		P_1P_1									
64/24	1.86E-01		2.04E-01									
128/48	5.94E-02	1.7	3.04E-02	2.7								
192/64	2.80E-02	1.9	1.45E-02	2.6								
256/128	1.75E-02	1.6	1.92E-03	2.9								
$\mathcal{O}3$	P_0P_2		P_1P_2		P_2P_2							
32 /16	5.09E-01		2.77E-01		5.59E-02							
64 /24	1.63E-01	1.6	8.97E-02	2.8	1.67E-02	3.0						
128/32	3.50E-02	2.2	2.91E-02	3.9	6.56E-03	3.2						
192/64	1.16E-02	2.7	2.07E-03	3.8	7.84E-04	3.1						
$\mathcal{O}4$	P_0P_3		P_1P_3		P_2P_3		P_3P_3					
32 /16	1.71E-01		1.95E-01		2.14E-02		1.77E-02					
64 /24	1.71E-02	3.3	4.95E-02	3.4	3.79E-03	4.3	2.46E-03	4.9				
128/32	1.28E-03	3.7	1.45E-02	4.3	8.95E-04	5.0	5.61E-04	5.1				
192/64	2.80E-04	3.7	5.16E-04	4.8	3.94E-05	4.5	2.07E-05	4.8				
$\mathcal{O}5$	P_0P_4		P_1P_4		P_2P_4		P_3P_4		P_4P_4			
32 /16	2.09E-01		9.85E-02		9.70E-03		5.22E-03		1.79E-03			
64 /24	2.30E-02	3.2	1.75E-02	4.3	1.18E-03	5.2	5.56E-04	5.5	2.24E-04	5.1		
128/32	1.16E-03	4.3	3.27E-03	5.8	2.09E-04	6.0	8.36E-05	6.6	4.36E-05	5.7		
192/64	1.63E-04	4.8	4.53E-05	6.2	7.23E-06	4.9	2.28E-06	5.2	1.75E-06	4.6		
$\mathcal{O}6$	P_0P_5		P_1P_5		P_2P_5		P_3P_5		P_4P_5		P_5P_5	
32 / 8	8.45E-02		5.50E-01		1.49E-01		6.22E-02		5.90E-02		2.76E-02	
64 /16	3.09E-03	4.8	8.72E-02	2.7	5.90E-03	4.7	1.73E-03	5.2	6.12E-04	6.6	4.69E-04	5.9
128/24	5.95E-05	5.7	1.46E-02	4.4	6.18E-04	5.6	1.39E-04	6.2	4.18E-05	6.6	3.72E-05	6.2
192/32	5.39E-06	5.9	2.39E-03	6.3	8.31E-05	7.0	2.17E-05	6.5	5.12E-06	7.3	4.99E-06	7.0

initial conditions together with the literature reference are all summarized in Table 2. Some of the test cases use the stiffened EOS, some of them only use a mixture of two ideal gases.

Since we want to validate our numerical method in multiple space dimensions, we solve all six shock tube problems on an unstructured triangular mesh in two space dimensions and Riemann problems RP1 and RP2 are even solved on an unstructured tetrahedral mesh in three space dimensions. The computational domain in 2D is $\Omega_{2D} = [-0.5; 0.5] \times [-\frac{5}{300}; \frac{5}{300}]$ and in 3D we use $\Omega_{3D} = [-0.5; 0.5] \times [-\frac{5}{300}; \frac{5}{300}]^2$. The characteristic mesh spacing is in all cases $h = 1/300$, corresponding to an equivalent one-dimensional resolution of 300 cells, which has also been used in [2] and [14]. The initial discontinuity is located at $x = 0$ and the final times are given in Table 2. For all test cases we use a third order WENO P_0P_2 scheme with reconstruction in characteristic variables. In x-direction we use transmissive boundaries and in all other directions periodic boundary conditions are imposed. We emphasize that in particular for the compressible Baer-Nunziato equations the use of reconstruction in conserved variables leads to a significant amount of spurious oscillations.

2D Results The results for the 2D computations are shown in Figs. 3 - 8. We show a sketch of the triangular mesh on the top left of each figure and a cut through the numerical solution on 300 equidistant points along the x-axis in the remaining sub-figures. For RP4, only the quantities shown are available as exact solution, see [32]. In general we can note a reasonable agreement between our numerical results and the exact reference solutions, which have been obtained from the articles [2,32,14] using a digitizer software.

3D Results The Riemann problems RP1 and RP2 have also been computed on an unstructured tetrahedral mesh in three space dimensions using a characteristic mesh spacing of $h = 1/300$. A cut through the mesh and the computational results are depicted together with the exact solution in Figs. 9 and 10. We note an excellent agreement with the exact solution and would underline that the results presented in this paper are, to our knowledge, the first computational results ever presented for the compressible Baer-Nunziato equations using higher than second order path-conservative WENO schemes on unstructured tetrahedral meshes in three space dimensions.

Table 2
Initial states left (L) and right (R) for the Riemann problems solved in 2D and 3D with the Baer-Nunziato model. Values for γ_i, π_i and the final time t_e are also given.

	ρ_s	u_s	p_s	ρ_g	u_g	p_g	ϕ_s	t_e
RP1 [14]:	$\gamma_s = 1.4$,	$\pi_s = 0$,	$\gamma_g = 1.4$,	$\pi_g = 0$				
L	1.0	0.0	1.0	0.5	0.0	1.0	0.4	0.10
R	2.0	0.0	2.0	1.5	0.0	2.0	0.8	
RP2 [14]:	$\gamma_s = 3.0$,	$\pi_s = 100$,	$\gamma_g = 1.4$,	$\pi_g = 0$				
L	800.0	0.0	500.0	1.5	0.0	2.0	0.4	0.10
R	1000.0	0.0	600.0	1.0	0.0	1.0	0.3	
RP3 [14]:	$\gamma_s = 1.4$,	$\pi_s = 0$,	$\gamma_g = 1.4$,	$\pi_g = 0$				
L	1.0	0.9	2.5	1.0	0.0	1.0	0.9	0.10
R	1.0	0.0	1.0	1.2	1.0	2.0	0.2	
RP4 [32]:	$\gamma_s = 3.0$,	$\pi_s = 3400$,	$\gamma_g = 1.35$,	$\pi_g = 0$				
L	1900.0	0.0	10.0	2.0	0.0	3.0	0.2	0.15
R	1950.0	0.0	1000.0	1.0	0.0	1.0	0.9	
RP5 [32]:	$\gamma_s = 1.4$,	$\pi_s = 0$,	$\gamma_g = 1.4$,	$\pi_g = 0$				
L	1.0	0.0	1.0	0.2	0.0	0.3	0.8	0.20
R	1.0	0.0	1.0	1.0	0.0	1.0	0.3	
RP6 [2]:	$\gamma_s = 1.4$,	$\pi_s = 0$,	$\gamma_g = 1.4$,	$\pi_g = 0$				
L	0.2068	1.4166	0.0416	0.5806	1.5833	1.375	0.1	0.10
R	2.2263	0.9366	6.0	0.4890	-0.70138	0.986	0.2	

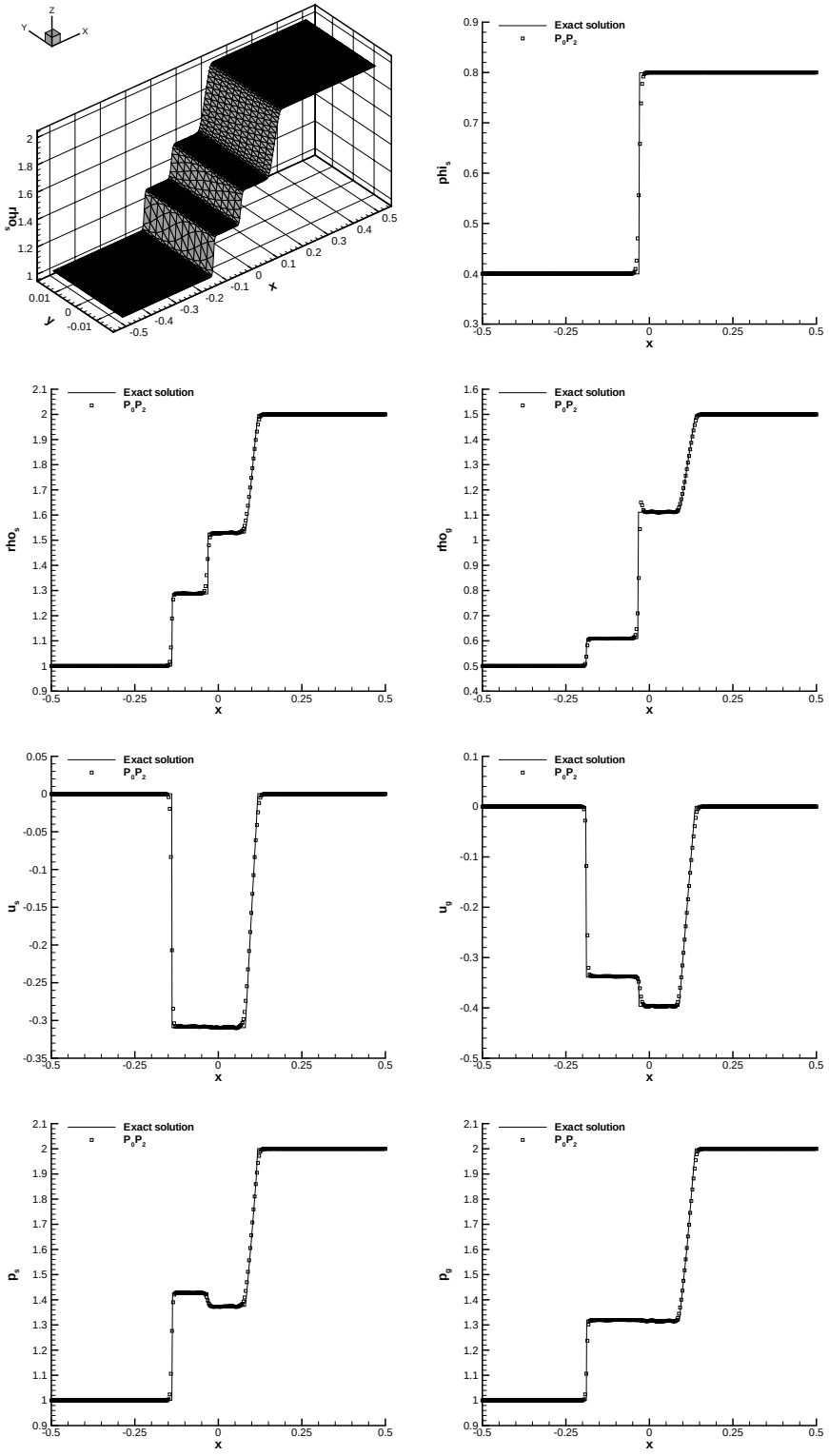

Fig. 3. Results for the 2D Riemann problem RP1 of the Baer-Nunziato model.

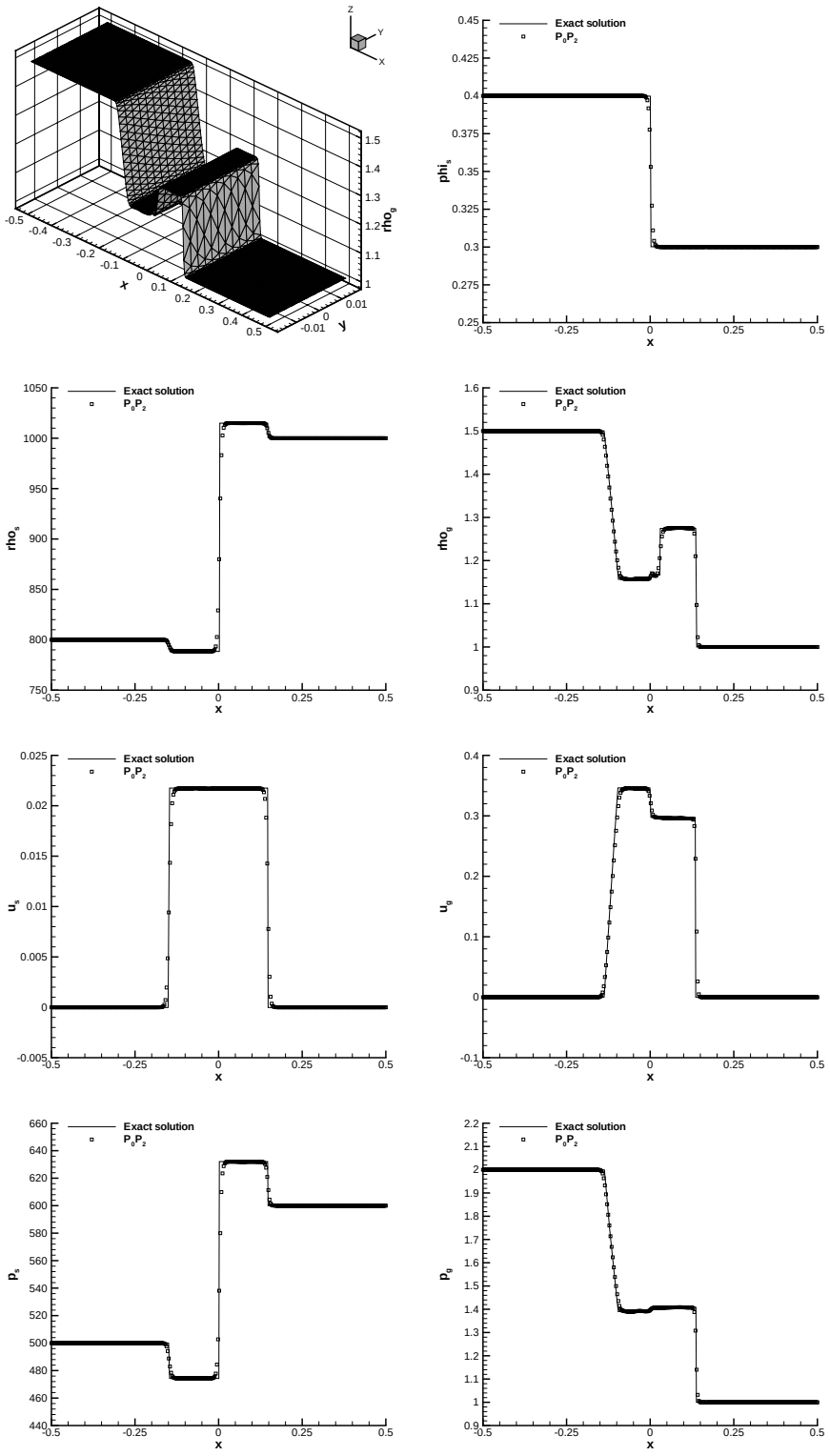

Fig. 4. Results for the 2D Riemann problem RP2 of the Baer-Nunziato model.

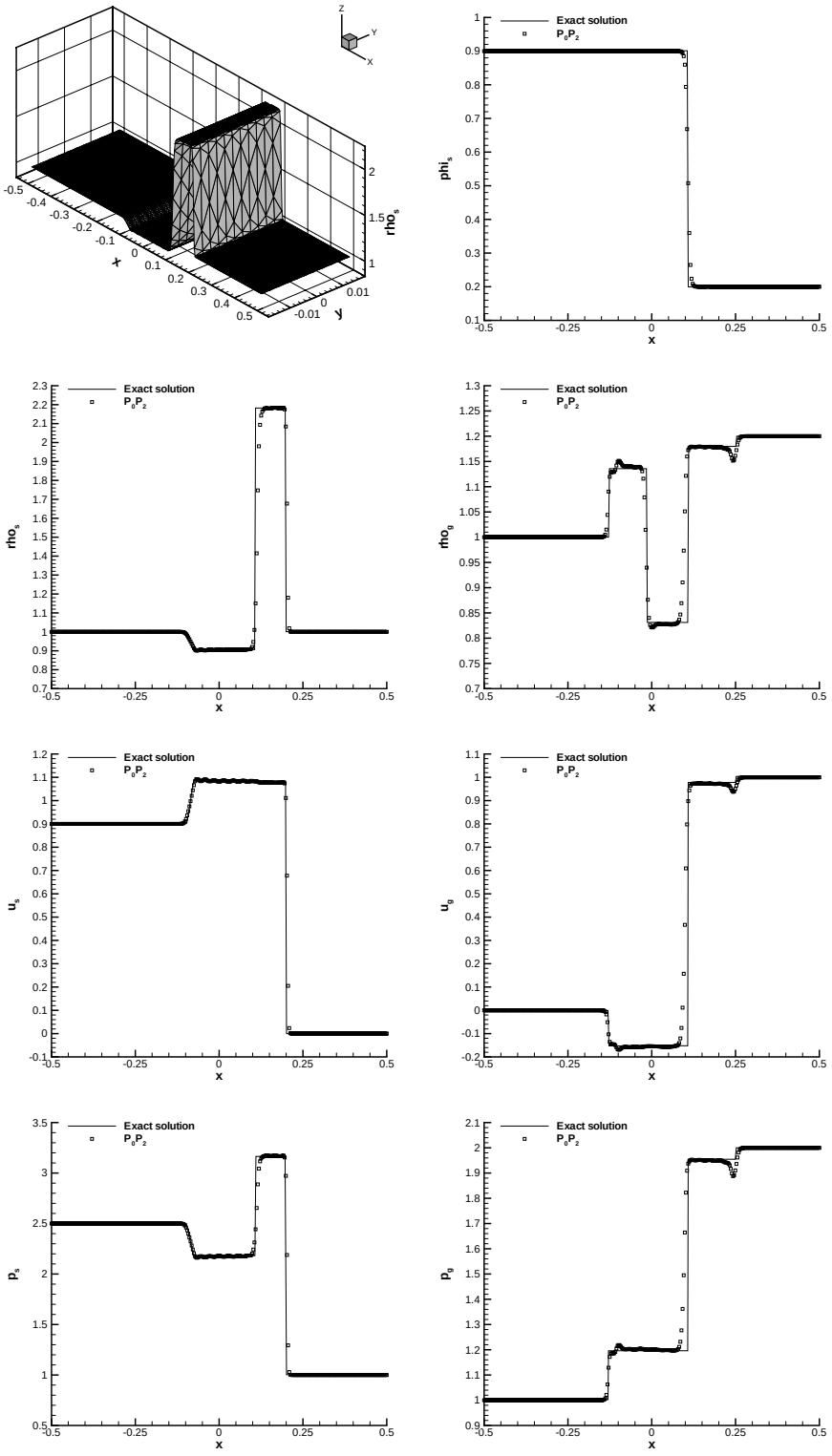

Fig. 5. Results for the 2D Riemann problem RP3 of the Baer-Nunziato model.

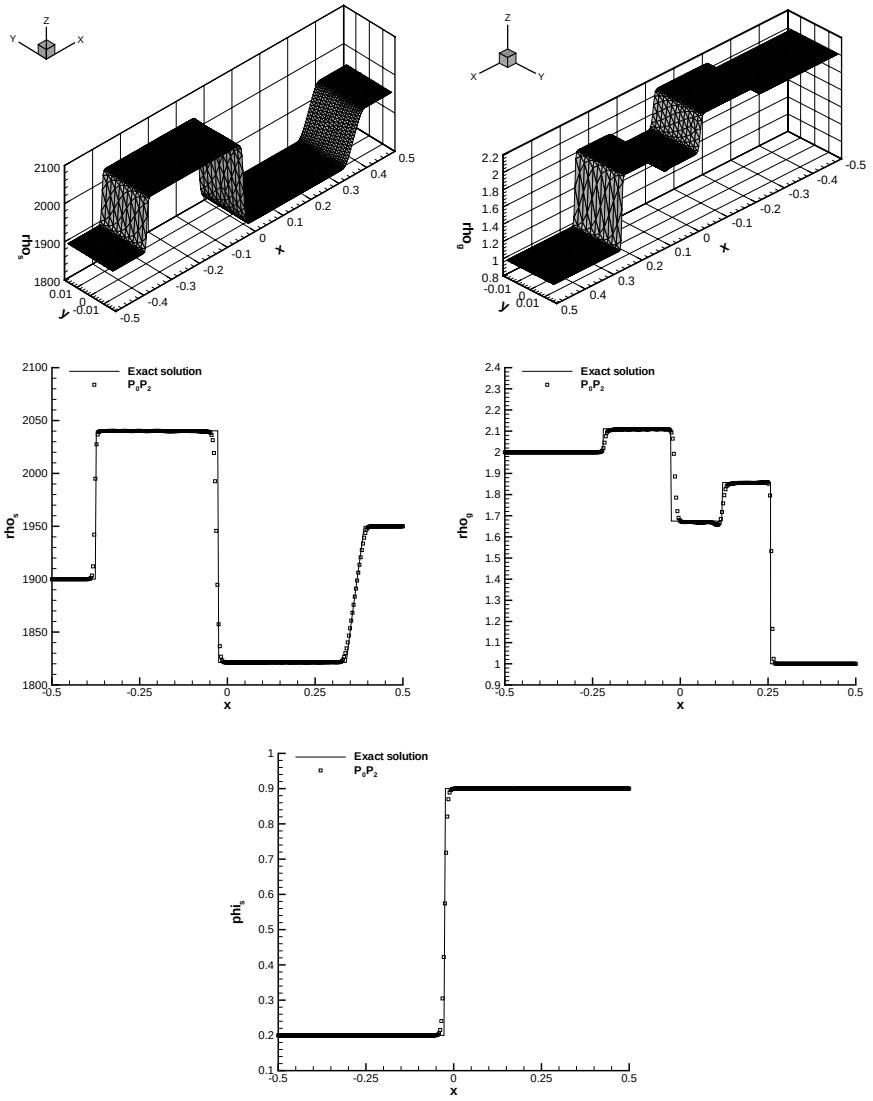

Fig. 6. Results for the 2D Riemann problem RP4 of the Baer-Nunziato model.

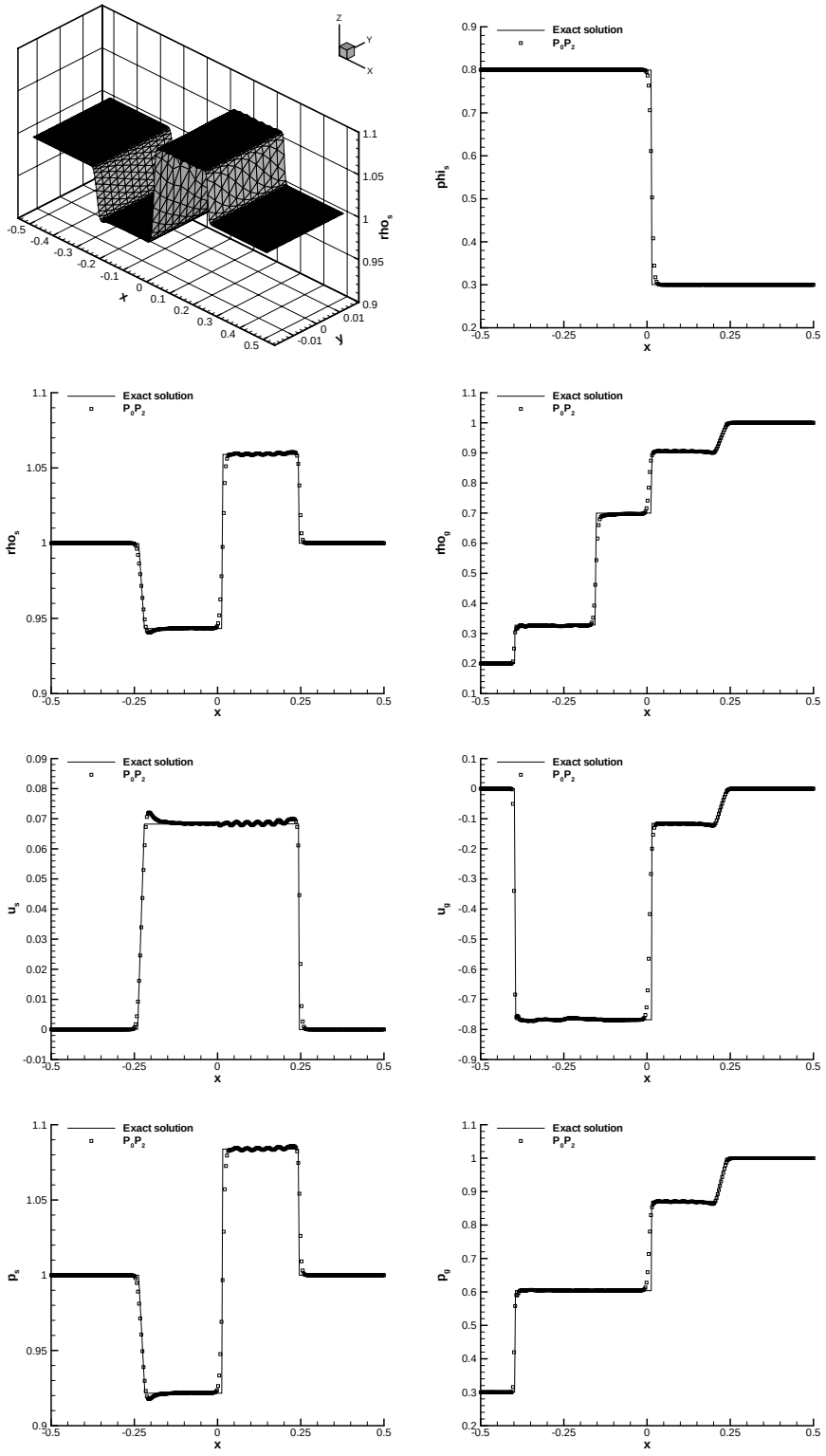

Fig. 7. Results for the 2D Riemann problem RP5 of the Baer-Nunziato model.

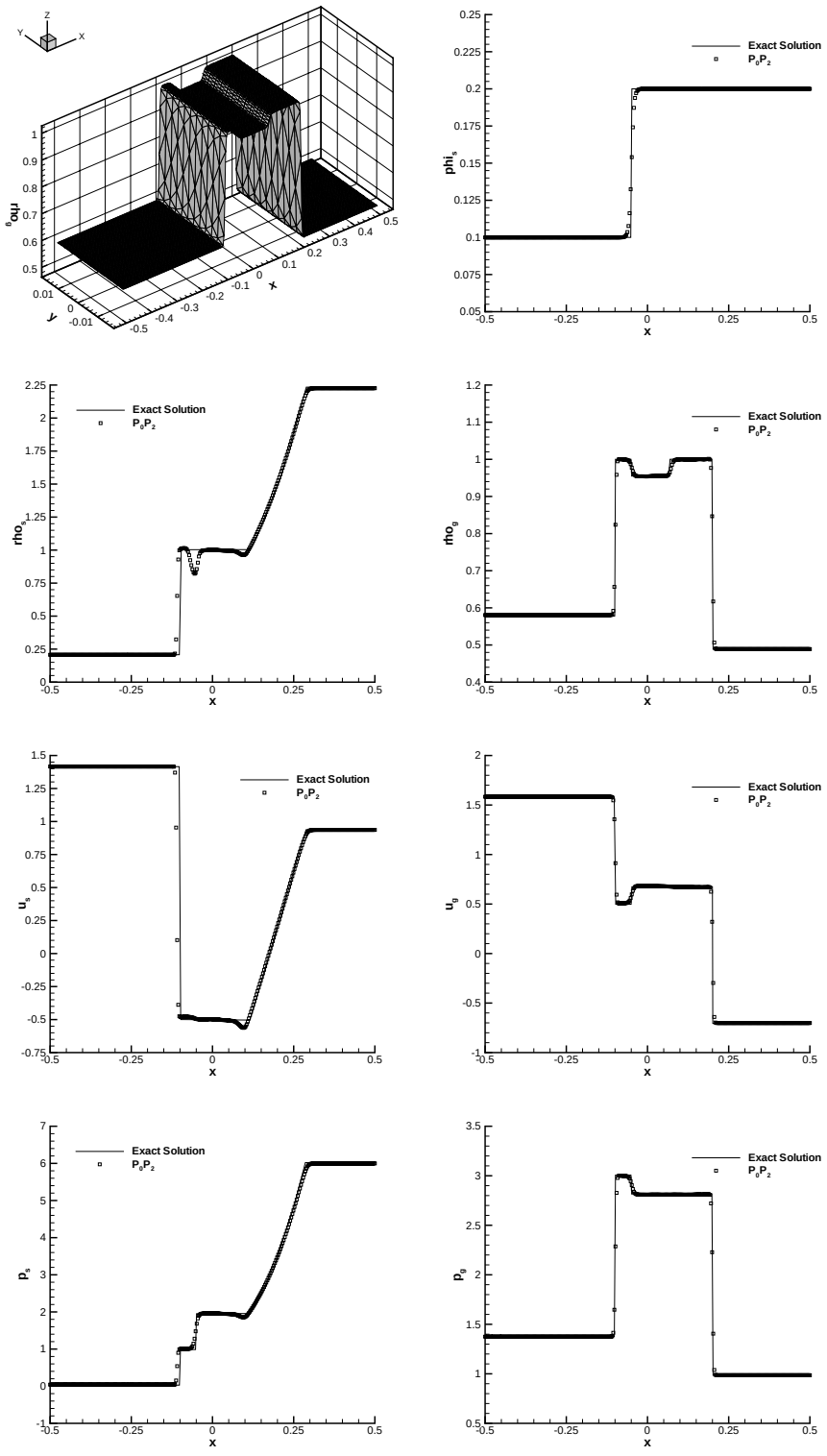

Fig. 8. Results for the 2D Riemann problem RP6 of the Baer-Nunziato model.

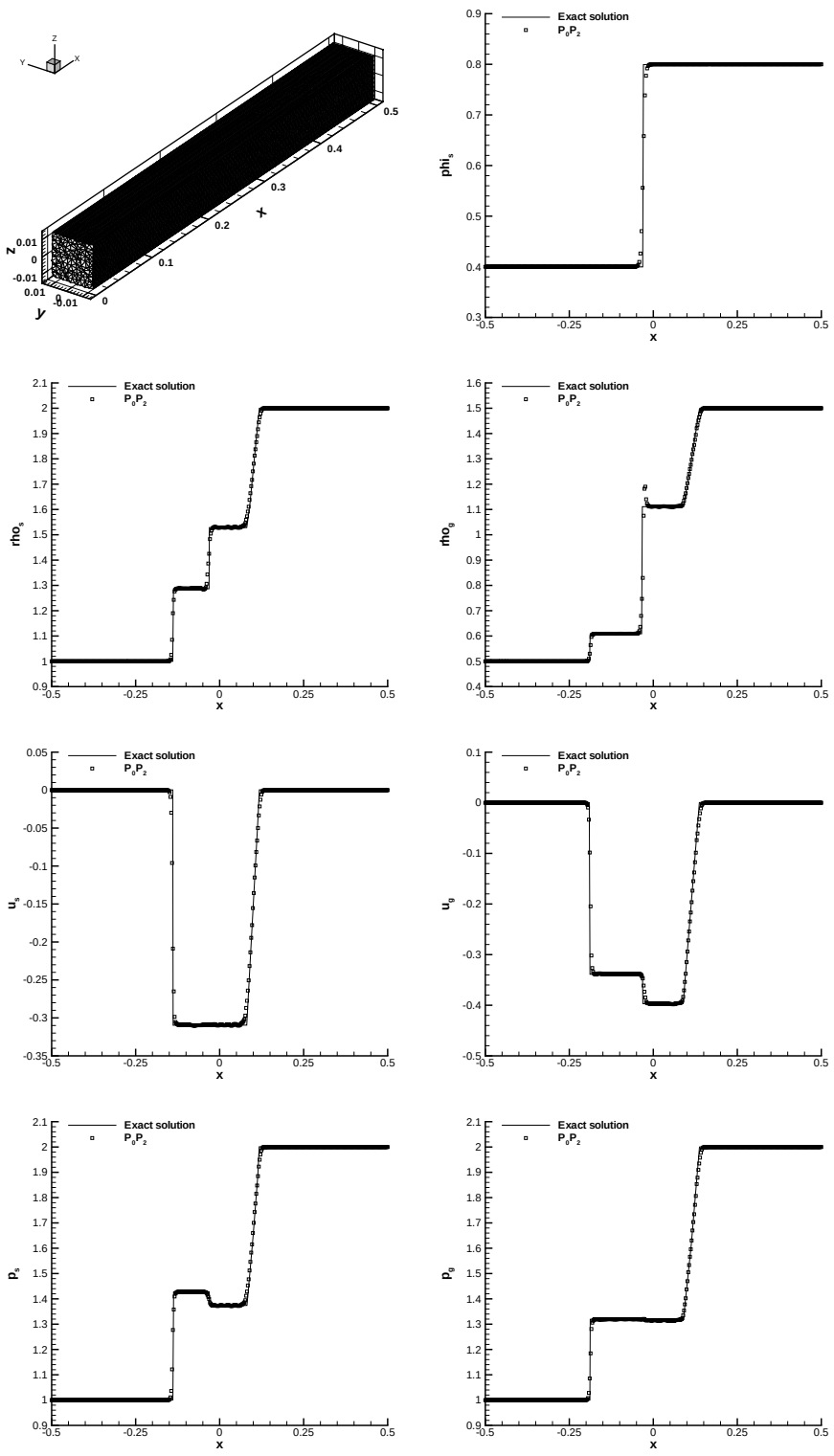

Fig. 9. Results for the 3D Riemann problem RP1 of the Baer-Nunziato model.

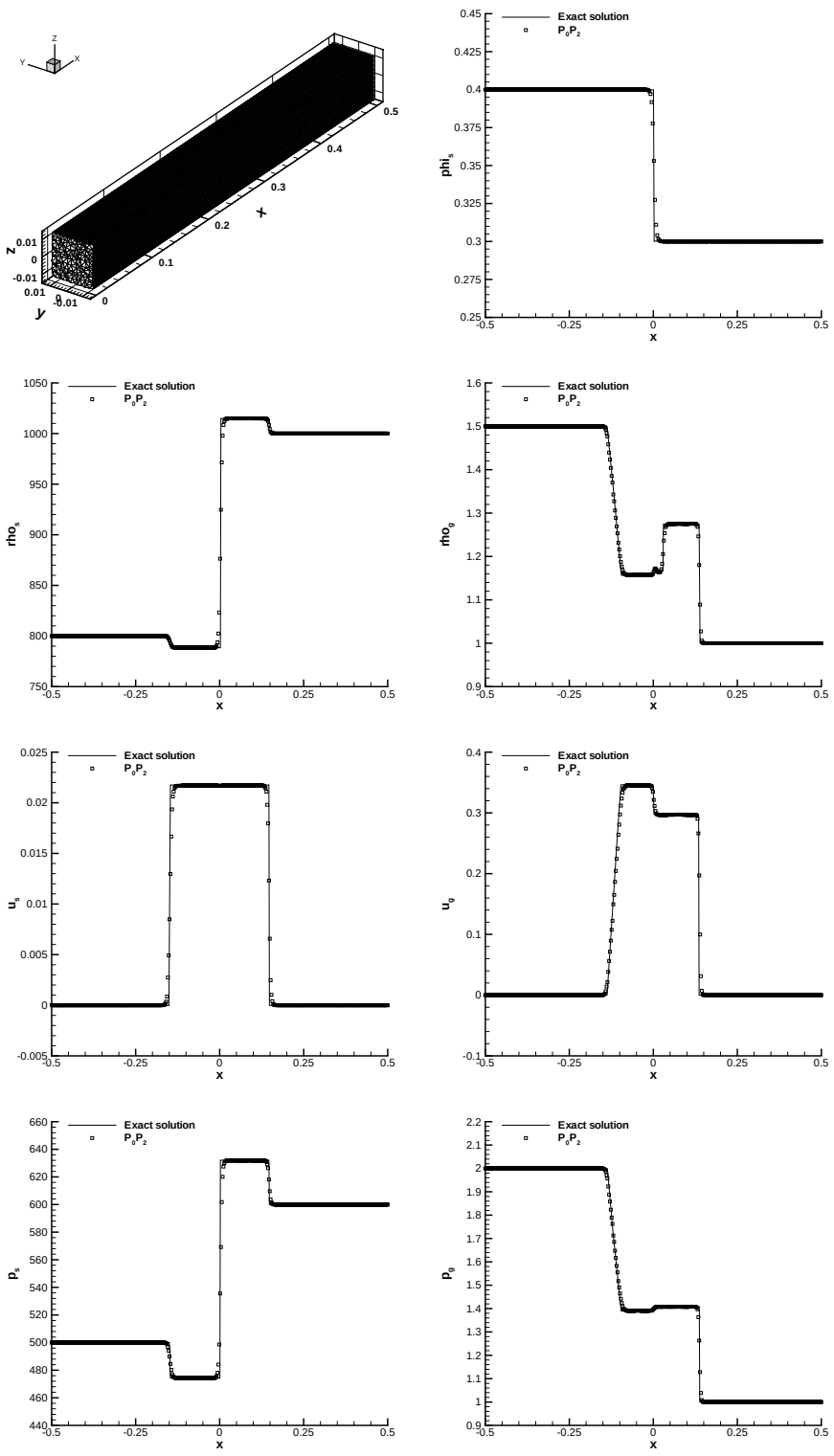

Fig. 10. Results for the 3D Riemann problem RP2 of the Baer-Nunziato model.

In this section we solve the compressible Baer-Nunziato equations in multiple space dimensions on a circular or spherical computational domain with radius $R = 0.8$. The initial condition is in all cases given by

$$W(\vec{x}, t = 0) = \begin{cases} W_i, & \text{if} \quad |\vec{x}| < 0.4, \\ W_o, & \text{otherwise.} \end{cases} \tag{45}$$

Computations are performed until $T = 0.18$. One can compute a very reliable reference solution for the two- and three-dimensional case solving the following equivalent (non-conservative) one-dimensional PDE in radial direction with geometric reaction source terms, where the parameter d is the number of space dimensions minus one and $\Delta u = (u_2^r - u_1^r)$:

$$\begin{aligned}
&\tfrac{\partial}{\partial t}\left(\phi_1\rho_1\right) + \tfrac{\partial}{\partial r}\left(\phi_1\rho_1 u_1^r\right) && = -\tfrac{d}{r}\left(\phi_1\rho_1 u_1^r\right), \\
&\tfrac{\partial}{\partial t}\left(\phi_1\rho_1 u_1^r\right) + \tfrac{\partial}{\partial r}\left(\phi_1\rho_1 \left(u_1^r\right)^2 + \phi_1 p_1\right) - p_2 \tfrac{\partial}{\partial r}\phi_1 && = -\tfrac{d}{r}\left(\phi_1\rho_1 \left(u_1^r\right)^2\right) + \lambda\Delta u, \\
&\tfrac{\partial}{\partial t}\left(\phi_1\rho_1\ E_1\right) + \tfrac{\partial}{\partial r}\left[\left(\phi_1\rho_1 E_1 + \phi_1 p_1\right) u_1^r\right] - p_2 u_1 \tfrac{\partial}{\partial r}\phi_1 && = -\tfrac{d}{r}\left[\left(\phi_1\rho_1 E_1 + \phi_1 p_1\right) u_1^r\right] + u_1^r\lambda\Delta u, \\
&\tfrac{\partial}{\partial t}\left(\phi_2\rho_2\right) + \tfrac{\partial}{\partial r}\left(\phi_2\rho_2 u_2^r\right) && = -\tfrac{d}{r}\left(\phi_2\rho_2 u_2^r\right)\ , \\
&\tfrac{\partial}{\partial t}\left(\phi_2\rho_2 u_2^r\right) + \tfrac{\partial}{\partial r}\left(\phi_2\rho_2 \left(u_2^r\right)^2 + \phi_2 p_2\right) + p_2 \tfrac{\partial}{\partial r}\phi_1 && = -\tfrac{d}{r}\left(\phi_2\rho_2 \left(u_2^r\right)^2\right) - \lambda\Delta u, \\
&\tfrac{\partial}{\partial t}\left(\phi_2\rho_2\ E_2\right) + \tfrac{\partial}{\partial r}\left[\left(\phi_2\rho_2 E_2 + \phi_2 p_2\right) u_2^r\right] + p_2 u_1 \tfrac{\partial}{\partial r}\phi_1 && = -\tfrac{d}{r}\left[\left(\phi_2\rho_2 E_2 + \phi_2 p_2\right) u_2^r\right] - u_1^r\lambda\Delta u, \\
&\tfrac{\partial}{\partial t}\phi_1 + u_1^r \tfrac{\partial}{\partial r}\phi_1 && = 0.
\end{aligned} \tag{46}$$

2D Computations. For our 2D computations we take a third order P_0P_2 WENO scheme with the multi-dimensional FORCE method as presented in this paper. An unstructured triangular mesh with a characteristic mesh spacing of $h = 1/500$ is used, leading to a mesh with 1,148,626 triangles.

For the first explosion problem (EP1) we choose the inner state W_i as the right state of RP5 and the outer state W_o as the left state of RP5 (see Table 2). The reference solution has been obtained solving the reduced one-dimensional system (46) with algebraic source terms that account for the radially symmetric geometry in 2D. The reference solution is computed using a second order TVD method together with a non-conservative Rusanov scheme on 10^5 cells. The numerical results are depicted in Fig. 11. We note that there are visible errors in the post-shock values present for the solid phase. This underlines the difficulty even of path-conservative schemes to converge to the correct weak solution of the non-conservative system (2) defined by the family of paths $\mathbf{\Psi}$. A detailed discussion of these problems can be found in [11]. However, the problems induced by the non-conservative system depend on the test case.

Therefore, we now solve a second explosion problem (EP2), whose initial condition is given by RP2 (see Table 2), where the left state of RP2 is chosen

to be the inner state W_i and the right state of RP2 is the outer state W_o. We solve the problem once without friction and once setting the friction parameter to $\lambda = 10$. The computational results together with the 1D reference solution are depicted in Fig. 12. For this test case, in contrast to the previous one, we note an excellent agreement between the reference solution and our 2D computation.

3D Computations. For the three-dimensional case, we solve again EP2, but this time on a computational domain in 3D that is composed by a half-sphere with radius $R = 0.8$ in the half-space $x > 0$. A characteristic mesh spacing of $h = 1/130$ is used, which already leads to a huge mesh containing 9,446,328 tetrahedrons. A segment of the mesh is depicted in Fig. 13. We use again a third order P_0P_2 WENO scheme. For more information about the implementation of the unstructured three-dimensional WENO method and its parallel performance see [18] and [19] for details. The computation has been performed on 510 CPUs of the HLRB2 supercomputer of the Leibniz supercomputing centre in München, Germany, and took about 12h wall-clock time. To our knowledge, this is the largest computation ever done with a path-conservative scheme of order greater than two on unstructured tetrahedral meshes in three-space dimensions. Also for the 3D case the reference solution has been computed solving the reduced 1D system with geometric reaction source terms (46). A comparison between our 3D computation and the reference solution is shown in Fig. 14. We observe an excellent agreement. All features of the solution are reasonably well resolved and our third order WENO method remains essentially non-oscillatory for this test case.

5.3 A Double Mach Reflection Problem for Compressible Two-Phase Flow

In this section we compute the double Mach reflection problem originally proposed by Woodward and Colella [39] for the compressible Euler equations. It consists of a discontinuity initially located at $x = 0$ moving with velocity $\sigma = 10$ to the right and hitting a 30° wedge. Using a segment path and imposing the right state, we obtain the left state behind the discontinuity from the generalized Ranking Hugoniot conditions (4). With $\gamma_s = 3.0$, $\pi_s = 2.0$, $\gamma_g = 1.4$ and $\pi_g = 0.0$, we obtain the following initial condition for the *conserved variables* in 2D: $W_L = (.4587156, 2.087156, 0, 11.31078, 4.285714, 35.35714, 0, 301.875, 0.25)$ and $W_R = (0.25, 0, 0, 0.875, 0.75, 0, 0, 1.3392857, 0.25)$. The state at rest ($W_R$) corresponds to $\rho_g = \rho_s = 1$ and $p_g = 1/\gamma_g$ and $p_s = 1$. We solve the problem on a computational domain that is depicted in Fig. 15. We impose transmissive boundary conditions in x-direction and solid walls are imposed on the upper and lower boundaries. The characteristic mesh spacing is set to $h = 1/400$, which leads to a mesh consisting of 3,284,840 triangles. A third order WENO

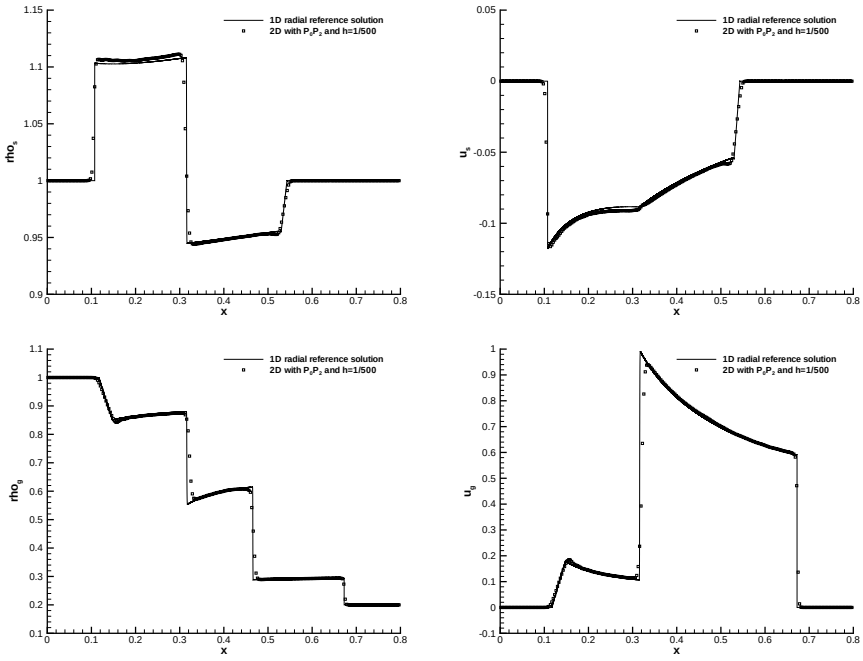

Fig. 11. Results for the first 2D explosion problem EP1. A cut along the x-axis is shown together with the 1D radial reference solution computed on 10^5 cells. Note the error in the solid phase. See [11] for a detailed discussion.

P_0P_2 scheme is used. The results obtained at $t = 0.2$ are shown in Fig. 15. We note that the initial discontinuity moves with the correct speed $\sigma = 10$, since it moves from its initial position $x = 0$ to its correct final position $x = 2$. For the gas phase (undisturbed sound speed $c_g = 1$) we find the typical flow structures present in the double Mach reflection problem at a Mach number of $M_g = 10$, see [39,34,23,19]. For the solid phase, the sound speed is larger ($c_s = 3$) and as a consequence the Mach number $M_s = \frac{10}{3}$ is lower. Hence, we only see the flow phenomena of classical Mach reflection. Since the solid volume fraction ϕ_s does not jump across non-linear waves, ϕ_s is a constant in space and time and therefore both phases completely decouple. In order to observe richer flow features, we modify the test case slightly in the next section, where we include a bubble in the initial condition that contains a larger solid volume fraction.

5.4 The Double Mach Reflection Problem with Shock-Bubble Interaction

The initial condition for the incident shock wave is exactly the same as in the previous section. The only difference in this section is that we now include a bubble with larger solid volume fraction in the state at rest. The bubble is located at $\vec{x} = (1.0, 1.5)$ and has a radius of $R = 0.5$. Within the bubble, the solid density is $\rho_s = 2$ and the solid volume fraction is $\phi_s = 0.75$. The pressures in the bubble are $p_g = 1/\gamma_g$ and $p_s = 1$ and the gas density is $\rho_g = 1$,

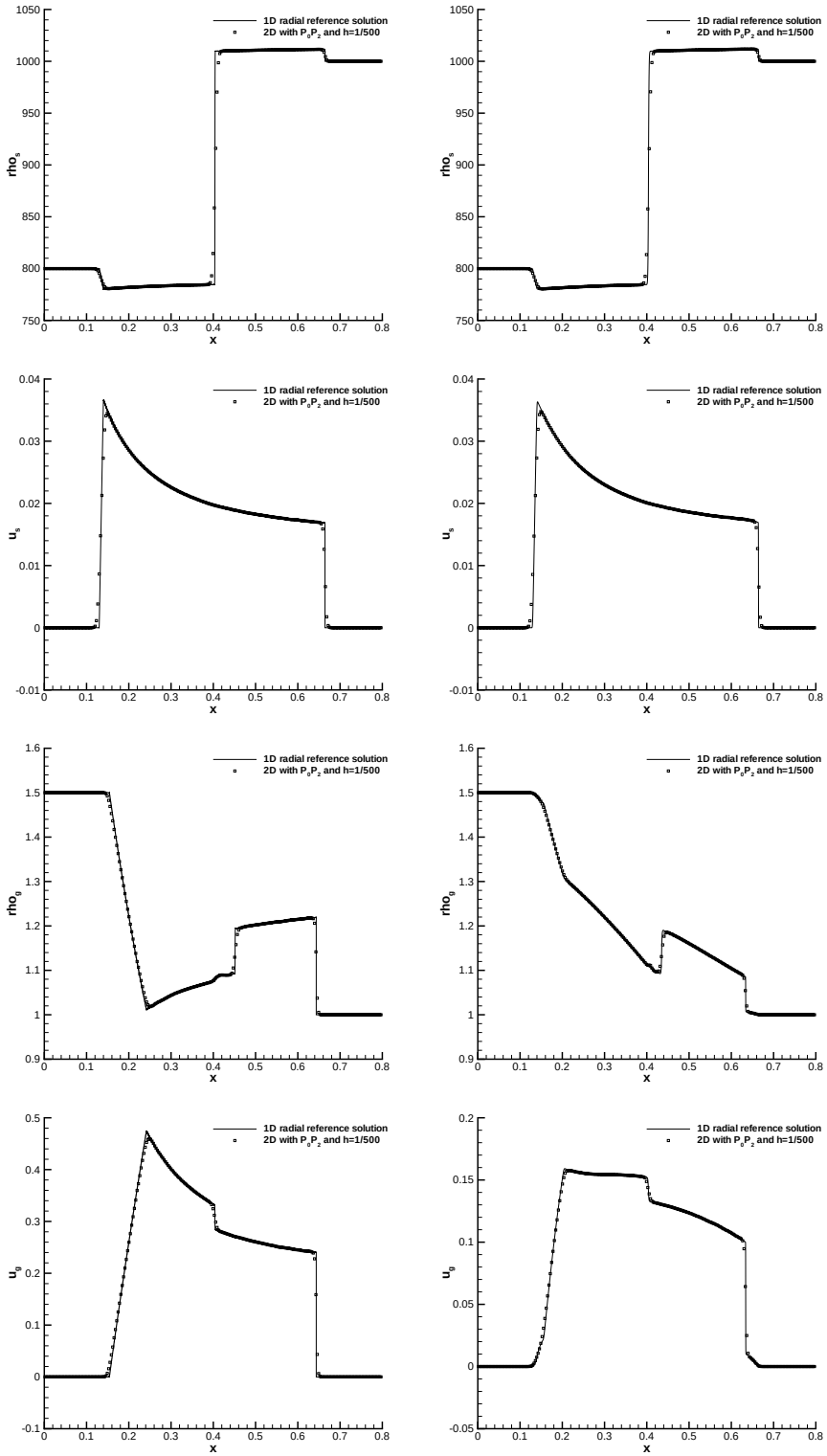

Fig. 12. Results for the second 2D explosion problem EP2. A cut along the x-axis is shown together with the 1D radial reference solution computed on 10^5 cells. Left column: no inter-phase friction. Right column: inter-phase friction with $\lambda = 10$.

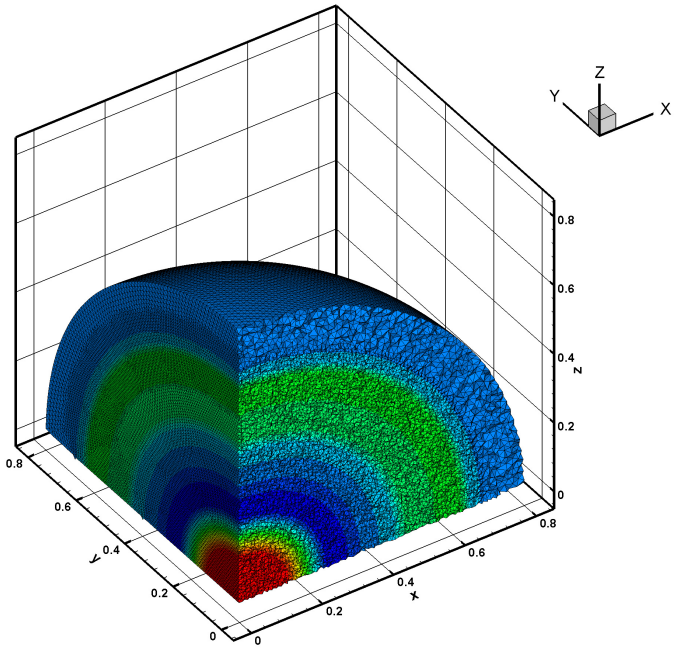

Fig. 13. Unstructured tetrahedral mesh for the 3D explosion problem. Only the segment with $x > 0$, $y > 0$ and $z > 0$ is shown. The contour colours represent ρ_g at $t = 0.18$.

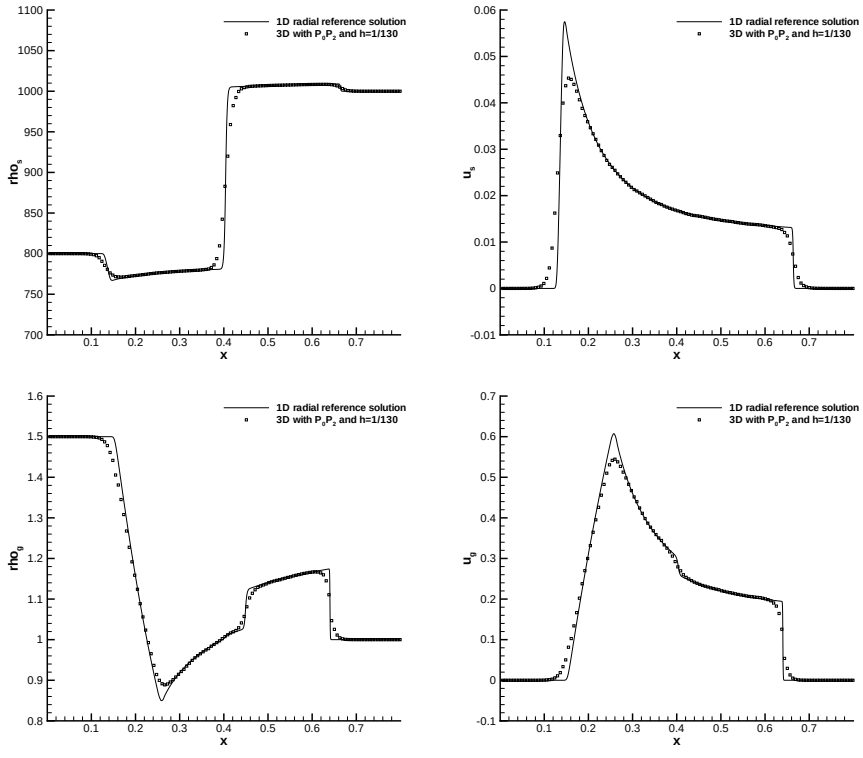

Fig. 14. Results for the 3D explosion problem. A cut along the x-axis is shown together with the 1D radial reference solution.

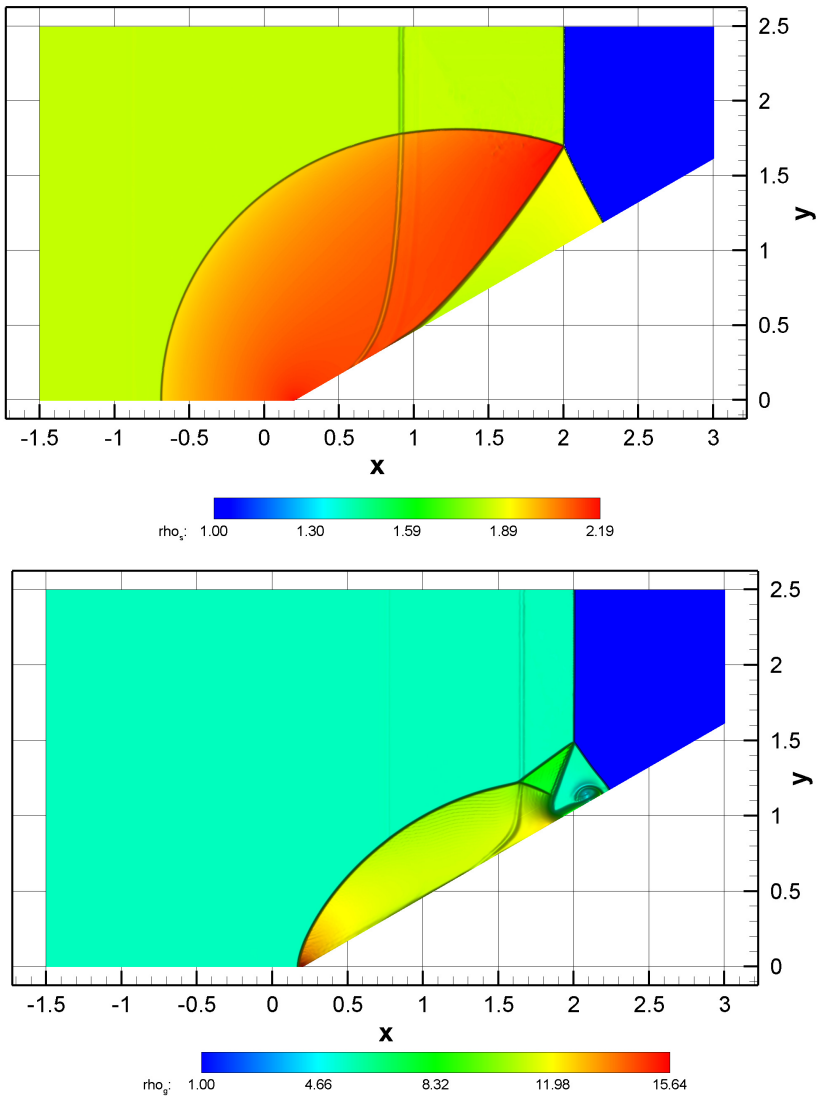

Fig. 15. Results for the two-phase double Mach reflection problem at $t = 0.2$. Top: solid density contours. Bottom: gas density contours.

as in the unperturbed state at rest (right state). We solve the problem on the same mesh with the same method until $t = 0.2$. The interaction of the incident shock wave with the bubble produces very complicated flow features and wave patterns that can be seen in Fig. 16. Immediately after the incident shock wave has hit the bubble, there is a reflected shock wave traveling to the left, that is then further reflected by the upper wall. The bubble is compressed, accelerated and moves to the right. The resulting solid contact and shear waves start to roll up. Of course we do not have any reference solution for this final test case, but the aim of this test is mainly to show the robustness of our high order method. It is able to handle simultaneously the strong discontinuities (shock Mach number $M_g = 10$) as well as the solid contact, the shear layers and the pressure waves.

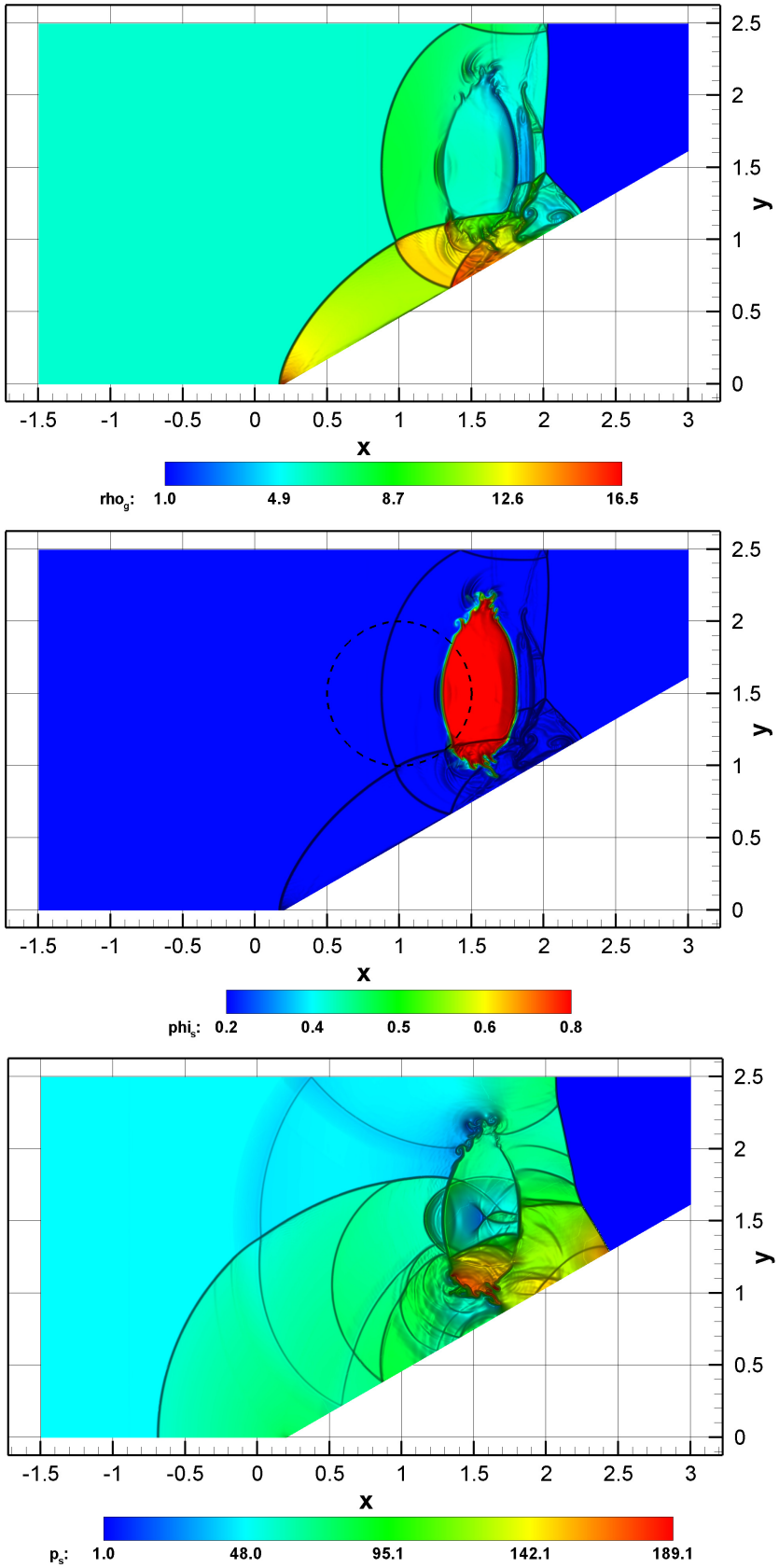

Fig. 16. Results for the two-phase double Mach reflection problem at $t = 0.2$, containing an initially circular bubble. Top: gas density contours. Middle: solid volume fraction and initial bubble geometry (dashed line). Bottom: solid pressure contours.

6 Conclusions

In this article we have presented a new class of arbitrary high order accurate *centered* one-step schemes for the solution of non-linear hyperbolic systems with non-conservative products and (stiff) source terms. The presented methods have been derived combining the recently developed $P_N P_M$ approach [15], which unifies finite volume and discontinuous Galerkin schemes in a more general framework, with the recently developed path-conservative schemes of Parés [28] and Castro et al. [10]. In contrast to the Roe-type $P_N P_M$ methods proposed in [16], which require the knowledge of the full eigenstructure of the system, the multi-dimensional FORCE schemes proposed in this article only need some elementary information about the geometry and the time-step and require just simple evaluations of the system matrix $\underline{\underline{A}}$, without knowing its eigenstructure. The extension of the FORCE method to non-conservative systems in multiple space-dimensions follows the guidelines given for the one-dimensional case in [12,6] and using the extension to general meshes proposed in [36]. The suggested centered schemes have been implemented in two and three space dimensions on unstructured triangular and tetrahedral meshes. Monotonicity has been assured using the WENO reconstruction presented in [18] and [19].

We have shown numerical convergence studies and some large-size test cases of the proposed schemes for the 2D and 3D Baer-Nunziato equations of compressible multi-phase flows. To our knowledge, problems of the size reported in this article have never been solved before using path-conservative schemes on unstructured triangular and tetrahedral meshes with schemes of order greater than two.

Due to the proposed centered framework on unstructured meshes, the schemes may have the potential to discretize very complicated non-conservative hyperbolic systems in arbitrarily complex geometries. These features may become of vital importance for example for the computation of chemically reacting compressible multi-phase flows in geometrically complex combustion chambers. In future work, we would like to simulate interactions between compressible liquids and gases including also viscous effects as well as surface tension.

7 Acknowledgments

The joint research presented in this paper was financed by the *Deutsche Forschungsgemeinschaft* (DFG) by the grant *DFG Forschungsstipendium* (DU 1107/1-1) as well as by the Italian ministry of research and education (MIUR) in the framework of the research project PRIN2007 and by the Spanish Gov-

ernment Research project MTM2006-08075.

References

[1] R. Abgrall. On essentially non-oscillatory schemes on unstructured meshes: analysis and implementation. *Journal of Computational Physics*, 144:45–58, 1994.

[2] N. Andrianov and G. Warnecke. The riemann problem for the baernunziato two-phase flow model. *Journal of Computational Physics*, 212:434–464, 2004.

[3] M.R. Baer and J.W. Nunziato. A two-phase mixture theory for the deflagration-to-detonation transition (DDT) in reactive granular materials. *J. Multiphase Flow*, 12:861–889, 1986.

[4] D. Balsara. Second-order accurate schemes for magnetohydrodynamics with divergence-free reconstruction. *The Astrophysical Journal Supplement Series*, 151:149–184, 2004.

[5] T.J. Barth and P.O. Frederickson. Higher order solution of the Euler equations on unstructured grids using quadratic reconstruction. *AIAA paper no. 90-0013*, 28th Aerospace Sciences Meeting January 1990.

[6] A. Canestrelli, A. Siviglia, M. Dumbser, and E.F. Toro. A well-balanced high order centered scheme for nonconservative systems: Application to shallow water flows with fix and mobile bed. *Advances in Water Resources*, doi:10.1016/j.advwatres.2009.02.006, 2009. in press.

[7] M.J. Castro, E. Fernández, A. Ferreiro, and C. Parés. Two-dimensional sediment transport models in shallow water equations. a second order finite volume approach over unstructured meshes. submitted.

[8] M.J. Castro, E. Fernández, A. Ferriero, J.A. García, and C. Parés. High order extensions of roe schemes for two dimensional nonconservative hyperbolic systems. *Journal of Scientific Computing*, 2008. In press.

[9] M.J. Castro, J.M. Gallardo, J.A. López, and C. Parés. Well-balanced high order extensions of godunov's method for semilinear balance laws. *SIAM Journal of Numerical Analysis*, 46:1012–1039, 2008.

[10] M.J. Castro, J.M. Gallardo, and C. Parés. High-order finite volume schemes based on reconstruction of states for solving hyperbolic systems with nonconservative products. applications to shallow-water systems. *Mathematics of Computations*, 75:1103–1134, 2006.

[11] M.J. Castro, P.G. LeFloch, M.L. Muñoz-Ruiz, and C. Parés. Why many theories of shock waves are necessary: Convergence error in formally path-consistent schemes. *Journal of Computational Physics*, 227:8107–8129, 2008.

[12] M.J. Castro, A. Pardo, C. Parés, and E.F. Toro. On some fast well-balanced first order solvers for nonconservative systems. submitted.

[13] B. Cockburn and C. W. Shu. The Runge-Kutta discontinuous Galerkin method for conservation laws V: multidimensional systems. *Journal of Computational Physics*, 141:199–224, 1998.

[14] V. Deledicque and M.V. Papalexandris. An exact riemann solver for compressible two-phase flow models containing non-conservative products. *Journal of Computational Physics*, 222:217–245, 2007.

[15] M. Dumbser, D. Balsara, E.F. Toro, and C.D. Munz. A unified framework for the construction of one-step finite-volume and discontinuous Galerkin schemes. *Journal of Computational Physics*, 227:8209–8253, 2008.

[16] M. Dumbser, M. Castro, C. Parés, and E.F. Toro. ADER schemes on unstructured meshes for non-conservative hyperbolic systems: Applications to geophysical flows. *Computers and Fluids*, doi:10.1016/j.compfluid.2009.03.008, 2009. in press.

[17] M. Dumbser, C. Enaux, and E.F. Toro. Finite volume schemes of very high order of accuracy for stiff hyperbolic balance laws. *Journal of Computational Physics*, 227:3971–4001, 2008.

[18] M. Dumbser and M. Käser. Arbitrary high order non-oscillatory finite volume schemes on unstructured meshes for linear hyperbolic systems. *Journal of Computational Physics*, 221:693–723, 2007.

[19] M. Dumbser, M. Käser, V.A Titarev, and E.F. Toro. Quadrature-free non-oscillatory finite volume schemes on unstructured meshes for nonlinear hyperbolic systems. *Journal of Computational Physics*, 226:204–243, 2007.

[20] M. Dumbser and C.D. Munz. Building blocks for arbitrary high order discontinuous Galerkin schemes. *Journal of Scientific Computing*, 27:215–230, 2006.

[21] J.M. Gallardo, C. Parés, and M.J. Castro. On a well-balanced high-order finite volume scheme for shallow water equations with topography and dry areas. *Journal of Computational Physics*, 227:574–601, 2007.

[22] A. Harten, B. Engquist, S. Osher, and S. Chakravarthy. Uniformly high order essentially non-oscillatory schemes, III. *Journal of Computational Physics*, 71:231–303, 1987.

[23] C. Hu and C.W. Shu. Weighted essentially non-oscillatory schemes on triangular meshes. *Journal of Computational Physics*, 150:97–127, 1999.

[24] V. P. Kolgan. Application of the minimum-derivative principle in the construction of finite-difference schemes for numerical analysis of discontinuous solutions in gas dynamics. *Transactions of the Central Aerohydrodynamics Institute*, 3(6):68–77, 1972. in Russian.

[25] G. Dal Maso, P.G. LeFloch, and F. Murat. Definition and weak stability of nonconservative products. *J. Math. Pures Appl.*, 74:483–548, 1995.

[26] M.L. Muñoz and C. Parés. Godunov method for nonconservative hyperbolic systems. *Mathematical Modelling and Numerical Analysis*, 41:169–185, 2007.

[27] A. Murrone and H. Guillard. A five equation reduced model for compressible two phase flow problems. *Journal of Computational Physics*, 202:664–698, 2005.

[28] C. Parés. Numerical methods for nonconservative hyperbolic systems: a theoretical framework. *SIAM Journal on Numerical Analysis*, 44:300–321, 2006.

[29] S. Rhebergen, O. Bokhove, and J.J.W. van der Vegt. Discontinuous Galerkin finite element methods for hyperbolic nonconservative partial differential equations. *Journal of Computational Physics*, 227:1887–1922, 2008.

[30] P.L. Roe. Approximate Riemann solvers, parameter vectors, and difference schemes. *Journal of Computational Physics*, 43:357–372, 1981.

[31] R. Saurel and R. Abgrall. A multiphase godunov method for compressible multifluid and multiphase flows. *Journal of Computational Physics*, 150:425–467, 1999.

[32] D.W. Schwendeman, C.W. Wahle, and A.K. Kapila. The riemann problem and a high-resolution godunov method for a model of compressible two-phase flow. *Journal of Computational Physics*, 212:490–526, 2006.

[33] A.H. Stroud. *Approximate Calculation of Multiple Integrals*. Prentice-Hall Inc., Englewood Cliffs, New Jersey, 1971.

[34] V.A. Titarev and E.F. Toro. ADER schemes for three-dimensional nonlinear hyperbolic systems. *Journal of Computational Physics*, 204:715–736, 2005.

[35] E.F. Toro and S. J. Billet. Centered TVD schemes for hyperbolic conservation laws. *IMA Journal of Numerical Analysis*, 20:44–79, 2000.

[36] E.F. Toro, A. Hidalgo, and M. Dumbser. FORCE schemes on unstructured meshes I: Conservative hyperbolic systems. *Journal of Computational Physics*. submitted to.

[37] I. Toumi. A weak formulation of roes approximate riemann solver. *Journal of Computational Physics*, 102:360–373, 1992.

[38] B. van Leer. Towards the ultimate conservative difference scheme V: A second order sequel to Godunov's method. *Journal of Computational Physics*, 32:101–136, 1979.

[39] P. Woodward and P. Colella. The numerical simulation of two-dimensional fluid flow with strong shocks. *Journal of Computational Physics*, 54:115–173, 1984.

[40] Y.T. Zhang and C.W. Shu. Third order weno scheme on three dimensional tetrahedral meshes. *Communications in Computational Physics*, 5:836–848, 2009.